VIROLOGY

Liver-expressed *Cd302* and *Cr1l* limit hepatitis C virus cross-species transmission to mice

Richard J. P. Brown[1,2]*, Birthe Tegtmeyer[2], Julie Sheldon[2], Tanvi Khera[2,3], Anggakusuma[2,4], Daniel Todt[2,5,6], Gabrielle Vieyres[2,7], Romy Weller[2], Sebastian Joecks[2], Yudi Zhang[2], Svenja Sake[2], Dorothea Bankwitz[2], Kathrin Welsch[2], Corinne Ginkel[2], Michael Engelmann[2,5], Gisa Gerold[8,9], Eike Steinmann[2,5], Qinggong Yuan[10,11], Michael Ott[10,11], Florian W. R. Vondran[12,13], Thomas Krey[13,14,15,16,17], Luisa J. Ströh[14], Csaba Miskey[18], Zoltán Ivics[18], Vanessa Herder[19], Wolfgang Baumgärtner[19], Chris Lauber[2,20], Michael Seifert[20], Alexander W. Tarr[21,22], C. Patrick McClure[21,22], Glenn Randall[23], Yasmine Baktash[24], Alexander Ploss[25], Viet Loan Dao Thi[26,27], Eleftherios Michailidis[27], Mohsan Saeed[26,28], Lieven Verhoye[29], Philip Meuleman[29], Natascha Goedecke[30], Dagmar Wirth[30,31], Charles M. Rice[26], Thomas Pietschmann[2,13,15]*

Hepatitis C virus (HCV) has no animal reservoir, infecting only humans. To investigate species barrier determinants limiting infection of rodents, murine liver complementary DNA library screening was performed, identifying transmembrane proteins Cd302 and Cr1l as potent restrictors of HCV propagation. Combined ectopic expression in human hepatoma cells impeded HCV uptake and cooperatively mediated transcriptional dysregulation of a noncanonical program of immunity genes. Murine hepatocyte expression of both factors was constitutive and not interferon inducible, while differences in liver expression and the ability to restrict HCV were observed between the murine orthologs and their human counterparts. Genetic ablation of endogenous *Cd302* expression in human HCV entry factor transgenic mice increased hepatocyte permissiveness for an adapted HCV strain and dysregulated expression of metabolic process and host defense genes. These findings highlight human-mouse differences in liver-intrinsic antiviral immunity and facilitate the development of next-generation murine models for preclinical testing of HCV vaccine candidates.

INTRODUCTION

Hepatitis C virus (HCV) chronically infects 71 million people worldwide, resulting in 400,000 deaths per year (*1*). Despite major advances in antiviral treatment, no vaccine for HCV is available, and with ca. 1.75 million new infections in 2015, virus transmission rates remain high (*2*). HCV can establish chronic infections in the human liver, causing progressive liver damage and leading to severe complications including cirrhosis and hepatocellular carcinoma. In general, viruses are usually well adapted to their host, and cross-species transmissions can be limited by host factor incompatibilities and restriction factors (*3*). Tropism and pathogenesis depend on exploitation of host factors supporting infection and evasion of cellular antiviral mechanisms (*4*, *5*). HCV naturally infects only humans, preventing studies of progressive immunopathogenesis or preclinical testing of novel therapeutics in an immunocompetent animal model. Recently, in attempts to address this problem, related viruses infecting diverse species have been repurposed as infection models for hepaciviruses (*6*–*9*) in their natural hosts. However, these viruses are substantially divergent from their human-infecting counterpart, HCV, limiting their usefulness for clinical infection research. Previous work only

[1]Division of Veterinary Medicine, Paul Ehrlich Institute, 63225 Langen, Germany. [2]Institute for Experimental Virology, Centre for Experimental and Clinical Infection Research, Twincore, Feodor-Lynen-Strasse 7, 30625 Hannover, Germany. [3]Department of Gastroenterology and Hepatology, Faculty of Medicine, University Hospital Essen, University of Duisburg-Essen, 45147 Essen, Germany. [4]Department of Research and Development, uniQure Biopharma, BV, Amsterdam, Netherlands. [5]Ruhr University Bochum, Faculty of Medicine, Department for Molecular and Medical Virology, Bochum, Germany. [6]European Virus Bioinformatics Center (EVBC), 07743 Jena, Germany. [7]Heinrich Pette Institute, Leibniz Institute for Experimental Virology, Hamburg, Germany. [8]Department of Physiological Chemistry, University of Veterinary Medicine Hannover, Bünteweg 17, 30559 Hannover, Germany. [9]Department of Clinical Microbiology, Virology and Wallenberg Center for Molecular Medicine (WCMM), Umeå University, 901 85 Umeå, Sweden. [10]Department of Gastroenterology, Hepatology and Endocrinology, Hannover Medical School, 30625 Hannover, Germany. [11]Twincore Centre for Experimental and Clinical Infection Research, Feodor-Lynen-Strasse 7, 30625 Hannover, Germany. [12]Department of General, Visceral, and Transplant Surgery, Hannover Medical School, 30625 Hannover, Germany. [13]German Centre for Infection Research (DZIF), Hannover-Braunschweig Site, Braunschweig, Germany. [14]Institute of Virology, Hannover Medical School, Hannover, Germany. [15]Cluster of Excellence RESIST (EXC 2155), Hannover Medical School, Carl-Neuberg-Straße 1, 30625 Hannover, Germany. [16]Center of Structural and Cell Biology in Medicine, Institute of Biochemistry, University of Luebeck, Luebeck, Germany. [17]Centre for Structural Systems Biology (CSSB), Hamburg, Germany. [18]Division of Medical Biotechnology, Paul Ehrlich Institute, 63225 Langen, Germany. [19]Department of Pathology, University of Veterinary Medicine Hannover, 30559 Hannover, Germany. [20]Institute for Medical Informatics and Biometry, Carl Gustav Carus Faculty of Medicine, Technische Universität Dresden, Dresden, Germany. [21]School of Life Sciences, Faculty of Medicine and Health Sciences, University of Nottingham, Nottingham, UK. [22]School of Life Sciences and NIHR Nottingham BRC, University of Nottingham, Nottingham, UK. [23]Department of Microbiology, The University of Chicago, Chicago, IL 60439, USA. [24]Instituto de Biología Integrativa de Sistemas (I2SysBio), Parc Científic de Barcelona, Carrer del Catedràtic Agustín Escardino 9, 46980 Paterna, Valencia, Spain. [25]Department of Molecular Biology, Princeton University, Princeton, NJ 08544, USA. [26]Laboratory of Virology and Infectious Disease, The Rockefeller University, New York, NY 10065, USA. [27]Schaller Research Group at Department of Infectious Diseases, Molecular Virology, Heidelberg University Hospital, Cluster of Excellence CellNetworks, Heidelberg, Germany. [28]Department of Biochemistry, Boston University School of Medicine, National Emerging Infectious Diseases Laboratories, Boston University, Boston, MA 02118, USA. [29]Laboratory of Liver Infectious Diseases, Ghent University, Ghent, Belgium. [30]Helmholtz Centre for Infection Research, Division Model Systems for Infection and Immunity, Inhoffenstraße 7, 38124 Braunschweig, Germany. [31]Department of Experimental Hematology, Hannover Medical School, 30625 Hannover, Germany.
*Corresponding author. Email: richard.brown@pei.de (R.J.P.B.); thomas.pietschmann@twincore.de (T.P.)

partially defined the species barrier determinants that restrict the HCV host range to humans. Ablation of innate immune responses, coupled with ectopic supplementation of human entry factors CD81 and occludin (OCLN), increases HCV permissiveness of murine hepatocytes in vitro (*10*) and in vivo (*11*, *12*). Despite this, viral replication remained low. These studies point to the existence of additional unknown barriers to increased HCV susceptibility in the murine liver. This knowledge gap has impeded development of murine models for this important human pathogen, causing a substantial disease burden globally.

RESULTS

Murine *Cd302* and *Cr1l* are pan-genotypic restrictors of HCV infection

This study aimed to identify restriction factors suppressing HCV replication in the murine liver. To this end, we screened a cDNA library generated from the liver of an interferon (IFN)–treated mouse. The library was packaged in lentiviral/VSV-glycoprotein–enveloped pseudoparticles and transduced into n4mBid cells (S0), followed by two rounds of selection (S2) with cell culture–derived HCV (HCVcc, strain Jc1) (Fig. 1A). The human n4mBid cell line is a genetically modified Huh-7.5 derivative with an HCV-triggered cell death phenotype: n4mBid cells are highly permissive for HCV but undergo apoptosis upon HCV replication due to NS3-4A protease-mediated cleavage of a modified Bid protein (*13*). Two rounds of selection with HCV were performed, and surviving cells were expanded after each round of selection. RNA sequencing (RNA-seq) profiling of cell population S0, the initial n4mBid cell population after delivery of the cDNA library, and cell population S2, the population of cells after two consecutive challenges with HCV, revealed 1 to 2% of reads mapped to the mouse transcriptome (fig. S1), representing the integrated cDNA library. The majority of these integrated genes were protein coding loci (fig. S1). Infection with Renilla luciferase (R-luc) reporter HCV (genotype 2a, strain Jc1) revealed that S2 cells were 200-fold less permissive for HCV when compared to S0, while susceptibility for human coronavirus R-luc infection (strain 229E) remained unaffected (Fig. 1B). To identify the determinants of this phenotype, comparative analyses of human cellular and lentivirally transduced mouse transcriptomes from S0 and S2 cell populations were performed. No depletion of known human HCV dependency factors was apparent (fig. S1), while enrichment of mRNAs representing a subset of integrated murine genes was observed. Ten murine genes met our inclusion criteria for enrichment [S2 reads per kilobase per million bases mapped (RPKM) value >100, $-\log_{10} P > 5$] (Fig. 1C, left) and were individually investigated via lentiviral overexpression and subsequent infection with firefly luciferase (F-luc) reporter HCV (strain Jc1) (Fig. 1C, right). Subsequently, we focused on the two most potent HCV restrictors: murine *Cd302* (also known as *Dcl-1* and *Clec13a*) and *Cr1l* [complement component (3b/4b) receptor 1–like; also known as *Crry*]. Both were strongly enriched during HCV selection and abundantly expressed in the S2 population—in addition, their ectopic expression reduced HCV infection by greater than 50%.

Infection of Huh-7.5 cells ectopically expressing either *mCr1l* or *mCd302* with R-luc HCV (strain Jc1) revealed a 10- or 50-fold reduction in intracellular relative light units (RLU) accumulation over a 4- to 96-hour time course, respectively, when compared to the control cell line (Fig. 1D). The level of restriction conferred by either *mCd302* or *mCr1l* was considerably greater than that observed for human *NOS2*, a described anti-HCV factor (*14*). Combined *mCd302*/*mCr1l* expression enhanced the antiviral effect, suggesting that these proteins may act in concert, with RLU counts 200-fold reduced compared to the control cell line (Fig. 1D). Next, we performed infections of murine restriction factor–expressing cell lines with a panel of R-luc reporter HCV chimeras, encoding core-NS2 from genotypes 1 to 7 and NS3-NS5B from strain JFH-1. These strains encompass the genetic and antigenic diversity apparent in the structural proteins from globally sampled HCV isolates. We observed varied but potent restriction of infection by all HCV genotypes (Fig. 1E). In general, in agreement with genotype 2a infections, combined *mCd302*/*mCr1l* restriction was more potent than either factor alone. Infection of Huh-7.5 cells overexpressing *mCd302* and *mCr1l* (individually or in combination) with nonreporter HCV (strain Jc1) revealed an identical restriction phenotype to that observed with reporter HCV (Fig. 1F): A marked reduction of both intracellular viral RNA (vRNA, top) or secreted virions (bottom) was apparent at 72 hours post-infection (hpi) when compared to control cells. To confirm that *mCd302* and *mCr1l* also restrict patient-derived primary isolates, we ectopically expressed human *SEC14L2* in Huh-7.5 cells, which was previously shown to facilitate the propagation of primary HCV isolates in tissue culture (*15*). Huh-7.5–*SEC14L2* cells supported infection with sera of patients infected with genetically diverse HCV subtypes (1a, 1b, and 3a), which could be suppressed with daclatasvir—an inhibitor of the HCV NS5A phosphoprotein. Combining ectopic *SEC14L2* expression with either *mCd302* or *mCr1l*, we observed that both murine factors restrict infection of Huh-7.5 cells with HCV patient isolates (Fig. 1G).

To investigate the breadth of *mCd302* and *mCr1l* antiviral restriction, we conducted infection assays using a divergent panel of viruses. The related flaviviruses dengue virus (DENV), West Nile virus (WNV), and yellow fever virus (YFV), which are all transmitted by mosquito vectors, were not impaired by *mCd302* and *mCr1l* overexpression. Similarly, infection with human respiratory syncytial virus (hRSV) and a zoonotic strain of the hepatotropic hepatitis E virus (HEV) was not significantly impeded (fig. S2), although a modest effect on HEV replication could be observed. Together, these data indicate that murine *Cd302* and *Cr1l* mediate a strong and cooperative antiviral effect against HCV.

Cd302 and *Cr1l* coexpression inhibits HCV cell entry

Cellular localization of overexpressed mCd302 and mCr1l in Huh-7.5 cells was investigated by flow cytometry and immunofluorescence staining, revealing distribution of both proteins throughout the cytosol and concentration of expression at the plasma membrane (Fig. 2A). To investigate whether HCV infection was impeded at an early stage of the viral life cycle, we infected cells with lentiviral pseudoparticles decorated with HCV envelope proteins (HCVpps) from different strains (Con1 and UKN2B2.8) and compared them to HCVcc infections (Fig. 2B). These data revealed an entry-specific effect only for *mCd302* but not for *mCr1l* alone. However, entry-specific restriction of *mCd302* was further enhanced by coexpression with *mCr1l*, indicating that both factors act cooperatively to impede HCVpp entry. The level of restriction on HCVpp entry was 10- to 20-fold less than that observed for HCVcc infection. This could be due to differences between authentic virions and HCVpps including differences in envelope glycoprotein membrane incorporation, envelope lipid composition, N-linked glycosylation, lipoprotein

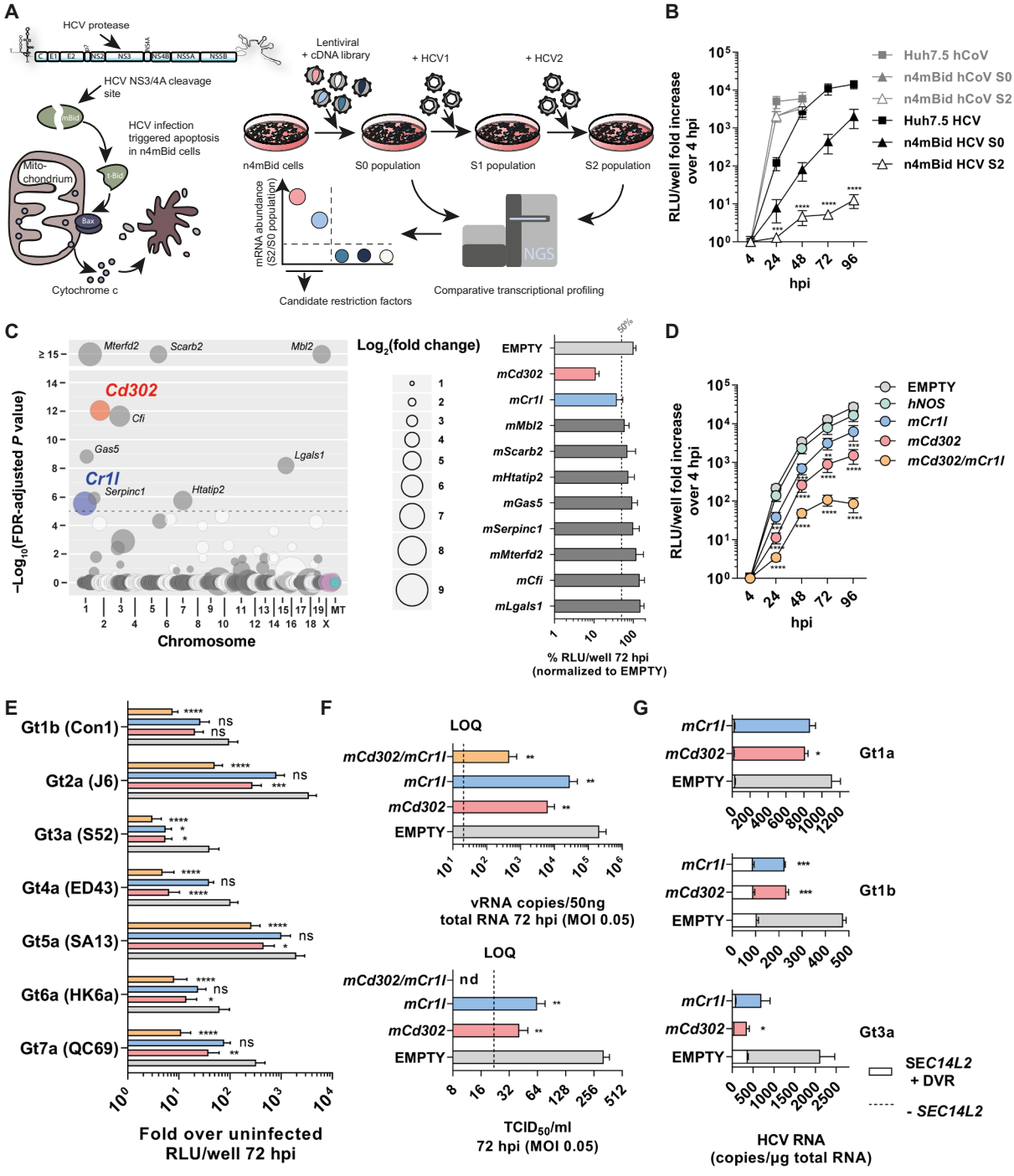

Fig. 1. Identification of murine restriction factors. (**A**) Library screening protocol. (**B**) Library-transduced cell line susceptibility to infection. Reporter HCV and human CoV-229E infections were conducted in parental Huh-7.5 cells, n4mBid S0 cells, and n4mBid S2 cells. Curves represent fold RLU increase over 4 hours post-infection (hpi), and values presented are means of $n = 4$ experiments ± the SEM. RLU, relative light units. (**C**) Identification of murine restriction factor candidates. Left: Genome-wide comparison of S0 and S2 integrated murine library ($n = 2$). Circles represent individual genes and are proportional to RPKM fold enrichment from S0 to S2, with associated *P* values plotted on the *y* axis. The dashed line represents the significance threshold. Right: HCV F-luc infection of Huh-7.5 cells ectopically expressing the indicated factors. Data presented were normalized to EMTPY values (100%) and represent the means of $n \geq 5$ experiments + SEM. (**D**) Restriction of reporter HCV infection. HCV R-luc infection of Huh-7.5 cells ectopically expressing the indicated genes. Curves represent fold RLU increase over 4 hpi, and values presented are means of $n \geq 4$ experiments ± SEM. (**E**) Restriction of all HCV genotypes. Indicated cell lines were infected with chimeric R-luc reporter viruses with color coding identical to (D). Data represent mean fold RLU increase over uninfected cells from $n = 3$ experiments + SEM. ns, not significant. (**F**) Restriction of nonreporter HCV. Infection of the indicated cells with WT HCV (strain Jc1) results in reduced vRNA and virion production. Mean data + SEM are plotted for $n = 5$ experiments. MOI: multiplicity of infection; $TCID_{50}$, mean tissue culture infectious dose; nd, none detected; LOQ, limit of quantification. (**G**) Restriction of patient-derived HCV. Cell lines ectopically expressing the indicated factors, with and without SEC14L2 coexpression, were infected with primary isolates of the indicated subtypes. Bars represent means of $n = 2$ technical replicates + SEM. DVR, daclatasvir. ****$P < 0.0001$, ***$P < 0.001$, **$P < 0.01$, and *$P < 0.05$.

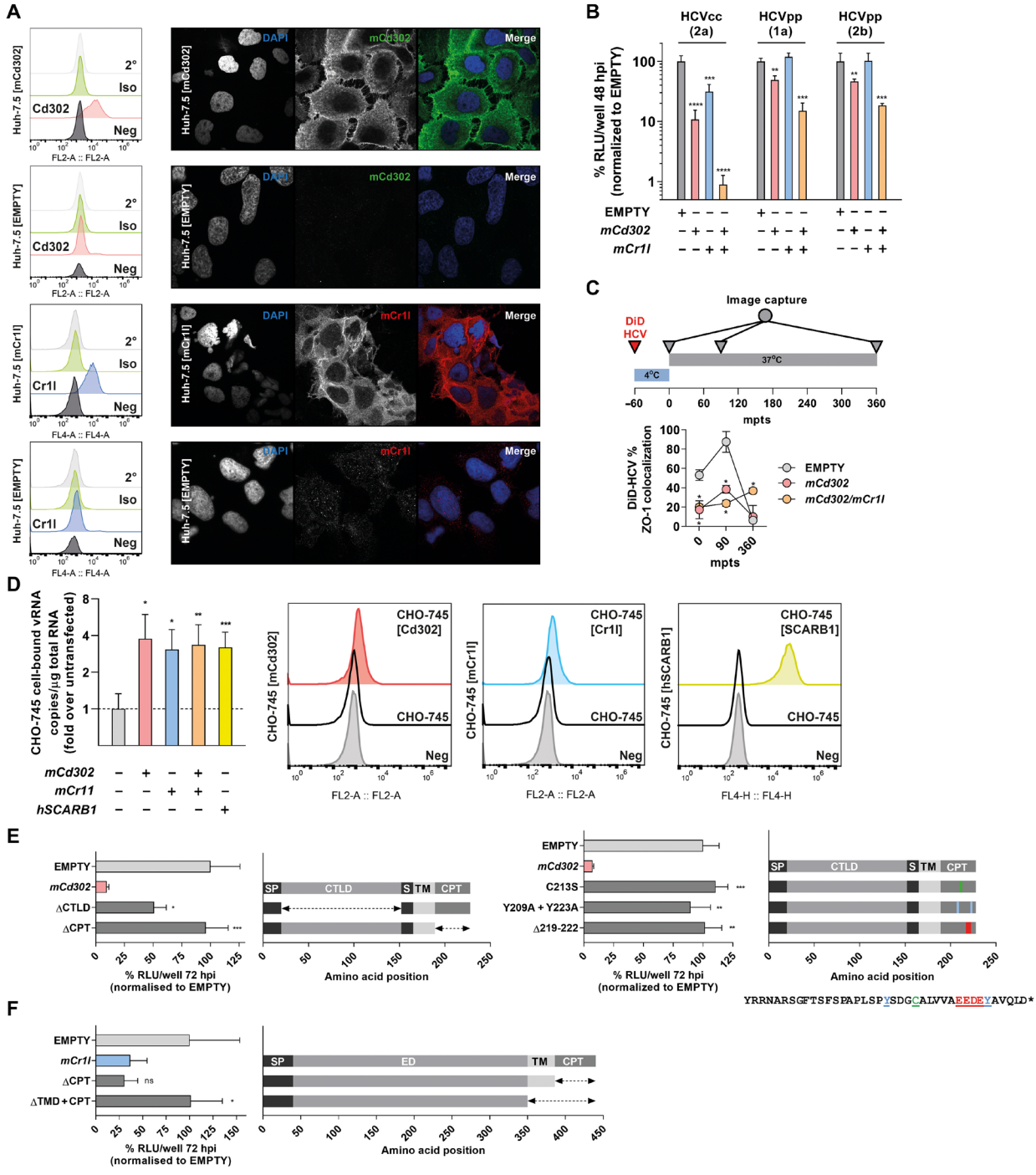

Fig. 2. Murine Cd302 and Cr1l impede HCV entry. (**A**) Cellular localization of murine Cd302 and mCr1l. Left: Surface expression of Cd302 or Cr1l determined by flow cytometry. 2°, secondary only; Iso, isotype control; Neg, unstained. Right: Immunofluorescence staining of the corresponding cell lines. (**B**) Cd302 and Cr1l impede entry of HCV pseudoparticles. Permissiveness of indicated cell lines to infection with HCVcc or HCVpp. Data are normalized to infection rates for EMPTY Huh-7.5 cells (100%) and represent means of $n = 3$ experiments + SEM. (**C**) Impaired HCV entry kinetics in polarized organoids. Top: Experimental procedure. Minutes post temperature shift (mpts). Bottom: Cd302 and Cr1l impede HCV translocation to the tight junction. Percentage of DiD-HCV located at tight junctions at the indicated time points. Data are normalized to total HCV particles per cell line at each individual time point (100%) and represent means of $n = 3$ experiments ± SD. (**D**) HCV directly binds Cd302 and Cr1l. Left: Binding of HCVcc to surface-expressed mCd302 and mCr1l. Data represent means + SEM from $n = 5$ experiments. Right: FACS analysis of nonpermeabilized CHO-745 cells overexpressing the indicated factors. Untransfected CHO-745 cells are highlighted in black, while unstained cells are shown in gray. (**E**) The C-type lectin domain and cytoplasmic tail of mCd302 combine to mediate HCV restriction. Protein cartoons denote domains of WT mCd302 with the position of engineered deletion or point mutants highlighted. Data represent the RLU means + SEM of $n = 5$ experiments normalized to infection rates in EMPTY cells. Mutated/deleted residues in the CPT are highlighted below. (**F**) The ectodomain of mCr1l mediates HCV restriction. Protein cartoon to the left denotes the relative functional domains of mCr1l. Data represent RLU means + SEM at 72 hpi of $n = 5$ experiments normalized to infection rates in EMPTY cells. ****$P < 0.0001$, ***$P < 0.001$, **$P < 0.01$, and *$P < 0.05$.

association, or the absence of secondary rounds of infection for HCVpps. Alternatively, the observed differences between HCVcc and HCVpp restriction may be due to additional targeting of post-entry stages, which are not recapitulated in the pseudoparticle infection assay.

To probe whether mCd302 and mCr1l impede HCV cell surface trafficking in polarized cells, we used a single-particle tracking assay. In this assay, Matrigel-polarized Huh-7.5 hepatoma cell organoids, which recapitulate the polarization of hepatocytes in vivo, were inoculated with purified, DiD-labeled HCV particles (*16*). Organoids transduced with an EMPTY vector, *mCd302*, or *mCr1l*/*mCd302* were inoculated with DiD-HCV at 4°C; unbound particles were washed away; and cells were shifted to 37°C to enable real-time visualization of bound particle trafficking to the tight junction (Fig. 2C, top). Organoids were fixed at multiple time points (minutes post temperature shift: mpts) and stained for ZO-1, a tight junction marker protein, DiD-HCV, and organoid nuclei. EMPTY vector cells showed a maximum colocalization of HCV with ZO-1 at 90 mpts consistent with previous data (*16*). However, organoids expressing *mCd302* or *mCr1l*/*mCd302* displayed significantly lower colocalization at 0 and 90 mpts (Fig. 2C, bottom). These data suggest a defect in trafficking to the tight junction, a crucial step in the HCV uptake process. Furthermore, while colocalization with control organoids drops off at 360 mpts, indicating that particles have internalized, DiD-HCV particles in *mCr1l*/*mCd302* organoids maintained colocalization with ZO-1, suggesting a possible internalization defect. Together, these data imply that mCd302 and mCr1l mediate their anti-HCV effect, in part, by disrupting steps of the complex entry cascade.

To investigate whether surface-expressed mCd302 and mCr1l proteins bind directly to HCV particles, we incubated HCVcc particles with either untransfected CHO-745 cells or CHO-745 cells transfected with *mCd302*, *mCr1l*, or *mCr1l*/*mCd302* plasmids. CHO-745 cells were used for the HCV attachment assay, because they lack endogenous expression of canonical HCV entry factors and are deficient in synthesis of proteoglycans due to a defect in xylosyltransferase activity, thus reducing nonspecific background binding. We used CHO-745 cells expressing the human HCV entry receptor *SCARB1*, which is known to bind virions directly, as a control (*17*–*19*). HCV was incubated with cells, followed by washing, RNA extraction, and quantification cell-bound vRNA by reverse transcription quantitative polymerase chain reaction (RT-qPCR) (Fig. 2D, left). Similar to cells expressing SCARB1, murine restriction factor expressing–cells exhibited ~3-fold more surface-bound HCV RNA when compared to untransfected CHO-745 cells, suggesting that both mCd302 and mCr1l can directly bind HCV, comparable to the levels seen for the HCV entry factor SCARB1. Surface localization of ectopically expressed factors was confirmed by flow cytometry. While cell surface localization of murine factors in CHO-745 cells was lower than that observed for human SCARB2, surface detection was apparent for both Cd302 and Cr1l (Fig. 2D, right).

Cd302 restriction is mediated by the C-type lectin domain and critical residues in the cytoplasmic tail

The murine *Cd302* gene encodes a 228–amino acid type I transmembrane protein containing a SP (SP; 20 amino acids), a CTLD (CTLD; 132 amino acids), a spacer region (S; 13 amino acids), a TM (TM; 24 amino acids), and a CPT (CPT; 39 amino acids) (*20*, *21*). To determine the mCd302 domain(s) important for the observed anti-HCV restriction, we initially generated two mCd302 domain deletion constructs: ΔCTLD and ΔCPT. While deletion of the CTLD partially ablated the restriction phenotype, truncation of the CPT completely ablated the inhibition of HCV infection (Fig. 2E, left). Expression and cell surface localization of the ΔCPT mutant protein were largely unaffected (fig. S3). In contrast, as the α-mCd302 antibody binds to the CTLD, the ability to detect this mutant protein was lost (fig. S3). Putative functional residues/motifs in the mCd302 CPT include a single cysteine residue (C213), which could serve as a putative palmitoylation site; two tyrosine residues (Y209 and Y223), which could be phosphorylated and involved in downstream signaling; and an EEDE acidic patch (219 to 222), which could serve as an internalization motif. Mutation/deletion of any of these critical residues completely destroyed the HCV restriction phenotype of Cd302 (Fig. 2E, right), while protein expression was unaffected (fig. S3). Cell surface expression of Cd302 CPT mutants was reduced compared to Cd302 wild type (WT), although still detectable (fig. S3).

The murine *Cr1l* gene encodes a 440–amino acid transmembrane protein containing an SP (40 amino acids), an ED (ED; 310 amino acids), a TM (36 amino acids), and a CPT (54 amino acids). In contrast to mCd302, ΔCPT of mCr1l had no effect on the capacity to restrict HCV infection, while deletion of the transmembrane domain and CPT together (ΔTM + CPT) disrupted plasma membrane incorporation and ablated HCV restriction (Fig. 2F). Together, these data identified the domains in each protein critical for the anti-HCV phenotype. Both the C-type lectin domain and the cytoplasmic tail are required for mCd302 to restrict HCV, with the cytoplasmic tail integral for restriction. In contrast, the ectodomain and membrane incorporation are required for mCr1l restriction.

Cd302/*Cr1l* restriction correlates with induction of a unique transcriptional program

Next, we explored whether *mCr1l*/*mCd302* restriction is dependent on IFN signaling. As both type I and type III IFNs signal via the Janus kinase–signal transducer and activator of transcription 1 (JAK/STAT1) signaling cascade, we treated ectopically expressing cell lines with the JAK/STAT inhibitor ruxolitinib, IFN (IFNα, subtype 2a), or a combination of both, followed by infection with HCV. JAK/STAT inhibition alone could not ablate HCV restriction in cells overexpressing *mCd302*/*mCr1l*, although the antiviral effect of IFN could be ablated and the infection phenotype could be rescued (Fig. 3A). These data indicate that murine *mCd302*/*mCr1l* restriction occurs independently of the JAK/STAT pathway.

To further investigate the mechanism of restriction, we used transcriptional profiling of Huh-7.5 cell lines ectopically expressing murine restriction factors (*mCd302*, *mCr1l*, and *mCd302*/*mCr1l*) and compared dysregulated genes signatures to control cell lines (EMPTY and *mCd302*ΔCPT), which are highly permissive for HCV infection. Levels of critical HCV entry factors *SCARBI*, *CD81*, *OCLN*, and *CLDN1* mRNA and cell surface protein expression were comparable in permissive and restricting cell lines. Likewise, mRNA levels of replication or assembly cofactor mRNAs *PI4KA*, *PPIA,* and *APOE* were also comparable (fig. S4). Analysis of differentially expressed genes (DEGs) in each cell line (when compared to the EMPTY cell line that is highly permissive for HCV infection) showed that HCV-permissive m*Cd302*ΔCPT cell transcriptomes were comparable to EMPTY cells, with relatively few DEGs detected (Fig. 3B). Of note, we observed increasing numbers of DEGs in *mCr1l*, *mCd302*,

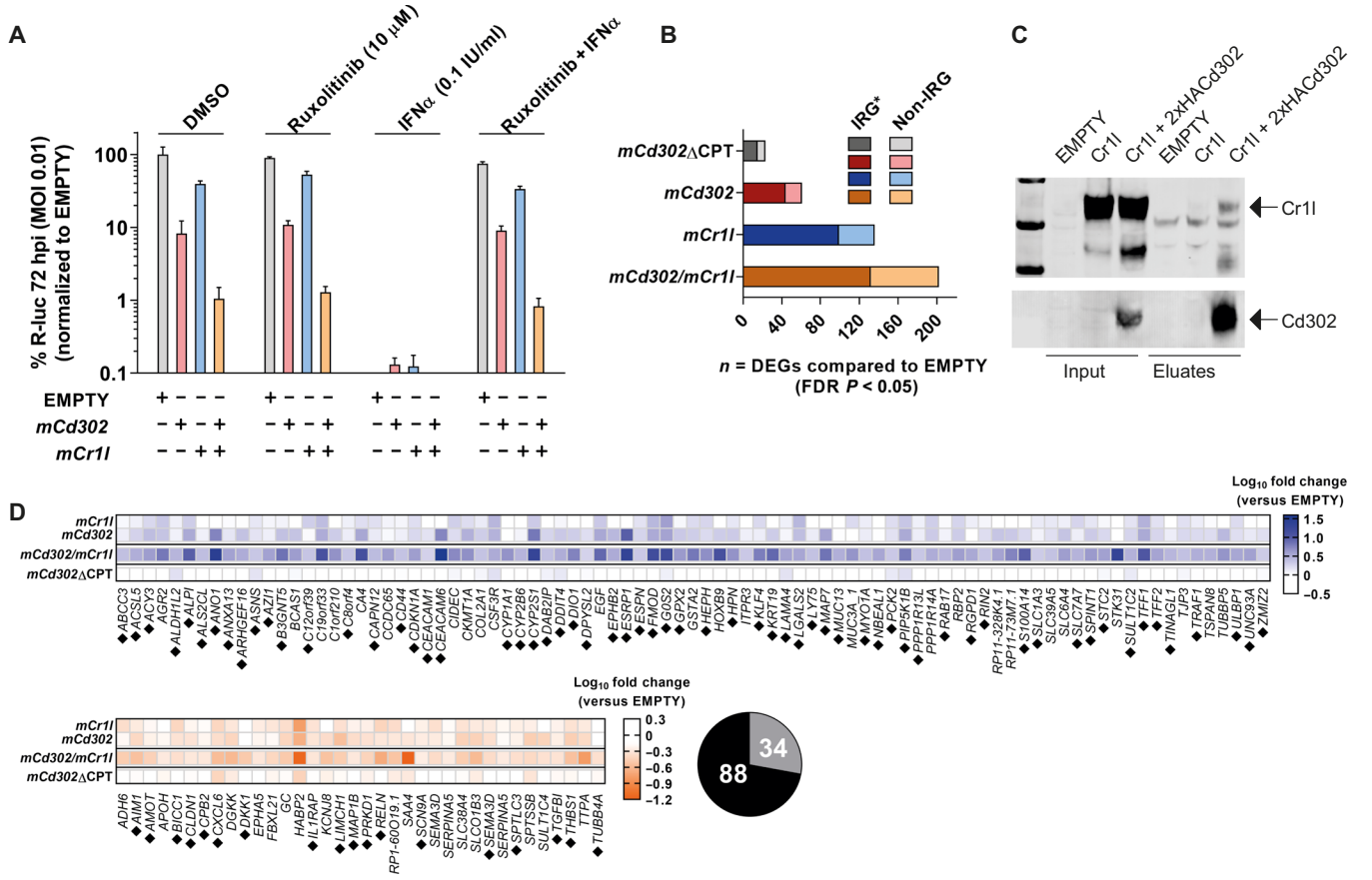

Fig. 3. Murine Cd302 and Cr1l interact and ectopic expression modulates the intrinsic Huh-7.5 transcriptome. (**A**) JAK/STAT inhibition does not ablate HCV restriction. Pretreatment of the indicated cell lines with JAK/STAT inhibitor (ruxolitinib), IFNα (subtype 2a), or ruxolitinib and IFNα in combination, followed by infection and readministration at 4 hpi. Data represent RLU means + SEM at 72 hpi of $n = 3$ experiments normalized to infection rates in EMPTY cells treated with a DMSO vehicle control. (**B**) Ectopic *mCd302* and *mCr1l* expression modulates the Huh-7.5 transcriptome. Data represent the number of differentially expressed genes (DEGs) (FDR $P < 0.05$) in each cell line when compared to EMPTY cells and are derived from RNA-seq of $n = 3$ replicates from nonidentical passages per cell line. *IRGs determined using Interferome v2.0 (*22*). (**C**) mCd302 and mCr1l proteins interact. Protein: Protein interaction of double HA-tagged mCd302 (2HACd302) and WT mCr1l was confirmed by immunoprecipitation of nuclear depleted cell lysates from double overexpressing cells via incubation with anti-HA resin followed by Western blotting detection with α-Cd302 and α-Cr1l antibodies. (**D**) Ectopic *mCd302* and *mCr1l* expression dysregulates a noncanonical gene program. Heatmap visualization of DEGs in *mCd302/mCr1l* cells described in (B) (FDR $P < 0.05$, final RPKM >1) with cellular mRNA expression of the indicated genes (RPKM) presented as fold change relative to EMPTY cells. Black diamonds associated with gene names represent IRGs. The proportion of IRGs is presented as a pie chart, with number of genes in each category inset. Black, IRG; and gray, non-IRG.

and *mCr1l*/*mCd302* cells, respectively, suggesting an additive or cooperative effect of overexpressing both factors in parallel, with ~200 DEGs apparent in *mCr1l*/*mCd302* cells (Fig. 3B). To investigate whether these two proteins physically interact, we performed immunoprecipitations. Coimmunoprecipitation of mCr1l with hemagglutinin (HA)–tagged mCd302 confirmed the mCd302-mCr1l interaction, indicating that both factors might bind each other and act cooperatively to mediate their combined potent anti-HCV phenotype (Fig. 3C). Stringent analyses of *mCr1l*- and *mCd302*-specific DEGs [false discovery rate (FDR) $P < 0.05$, only transcripts with RPKM >1 included] revealed a program of dysregulated genes in *mCd302* cells, which was further enhanced by coexpression with *mCr1l* (Fig. 3D). Cells ectopically expressing *mCd302*ΔCPT exhibited minimal DEGs, suggesting that *mCr1l*/*mCd302*-dependent transcriptional changes are dependent on the CPT of mCd302. In many cases, ectopic expression of *mCr1l* and *mCd302* individually up-regulated the same target gene and concomitant expression of both *mCr1l*/*mCd302* that further boosted expression of these targets (e.g., *ACY3*, *ALPI*, *C19orf33*, and *TFF1*), underpinning cooperativity between *mCr1l* and *mCd302* in transcriptional regulation of cellular genes. The majority of *mCr1l*/*mCd302*-specific DEGs (88 of 122) represented IFN-regulated genes (IRGs) (*22*). These data indicate that overexpression of *mCr1l*/*mCd302* results in the dysregulation of a specific subset of antiviral genes, which likely contributes an intrinsic anti-HCV phenotype.

Cd302 and *Cr1l* are constitutively expressed in murine hepatocytes and not induced by IFN

We next investigated whether murine hepatocytes express these identified restriction factors. Transcriptional profiling of total mouse livers and plated primary mouse hepatocytes (PMHs) from multiple standard laboratory strains revealed abundant expression of *mCd302* and *mCr1l* mRNA transcripts, comparable to well-characterized hepatocyte-specific transcripts (Fig. 4A). In contrast, brain- or lung-specific mRNAs were either barely detectable or completely absent. We observed constitutive expression of mCd302 and mCr1l proteins in primary murine hepatocytes by immunofluorescence

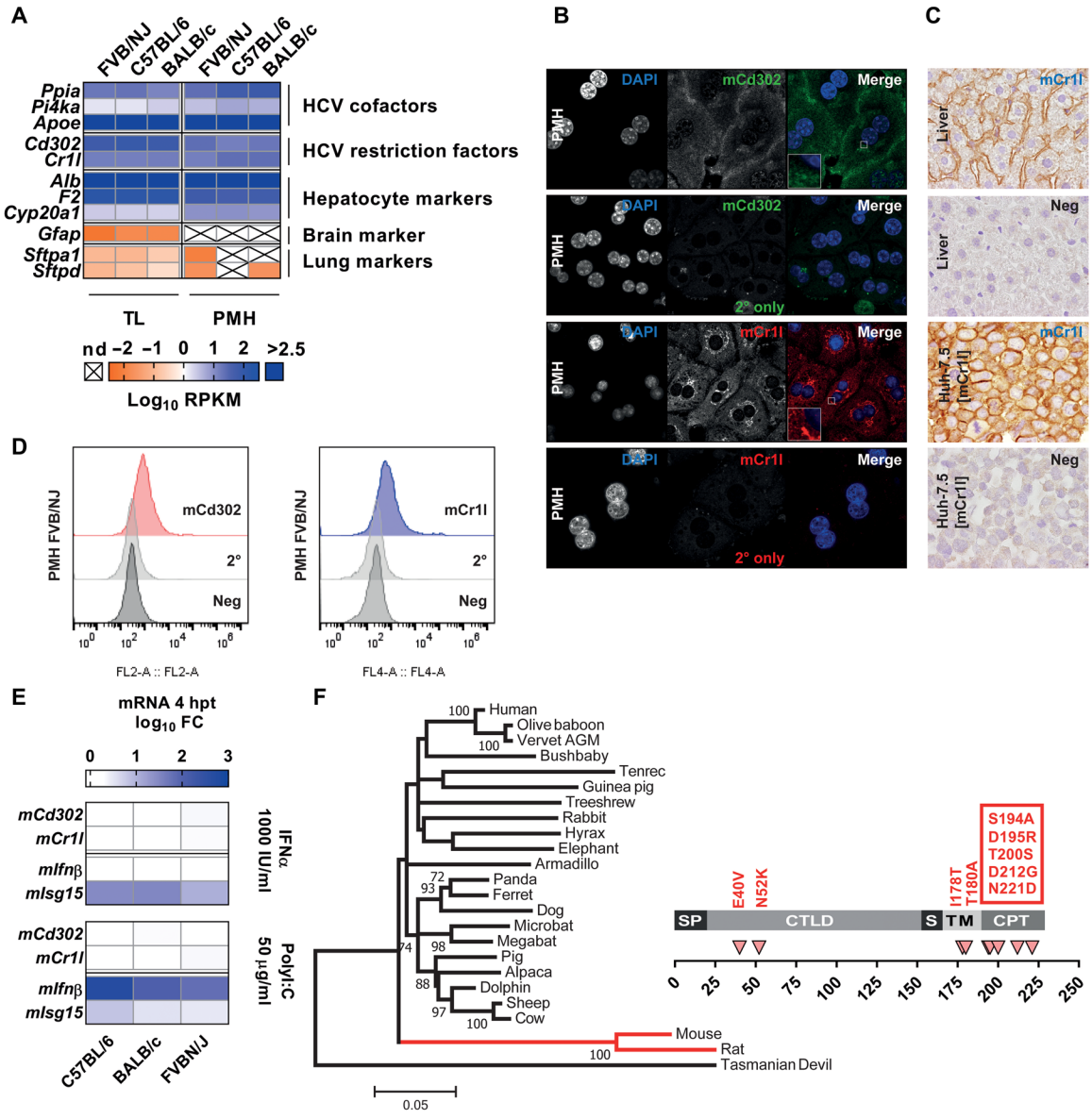

Fig. 4. *mCd302* and *mCr1l* are constitutively expressed in murine hepatocytes. (**A**) High intrinsic expression of *mCd302* and *mCr1l* mRNA in murine livers and hepatocytes. Intrinsic mRNA expression of selected genes present in total liver (TL) and plated primary mouse hepatocytes (PMHs) from the indicated mouse strains. Cells with X represent genes with no detectable expression (RPKM = 0). (**B**) Cellular localization of mCd302 and mCr1l proteins in murine hepatocytes. Immunofluorescence analysis of α-mCd302 or α-mCr1l antibody staining on plated PMHs determined by confocal microscopy with secondary only antibody staining controls. Insets magnify the perinuclear concentration of both proteins. (**C**) In situ staining of mCr1l in mouse liver slices. Immunohistochemical staining of mCr1l in murine liver slices versus unstained and pelleted Huh-7.5 [mCr1l] controls. (**D**) Cell surface localization of mCd302 and mCr1l on mouse hepatocytes. FACS staining of nonpermeabilized mouse hepatocytes with α-mCd302 or α-mCr1l antibodies, compared to secondary antibody only staining and unstained controls. (**E**) m*Cd302* and m*Cr1l* mRNA are not inducible. Heatmaps showing fold change (FC) in mRNA expression of candidate genes in PMHs derived from the indicated mouse strains. PMHs were either untreated or treated with IFNα2a or PolyI:C. Fold regulation was compared to *Ifn*β or *Isg15* induction. Four hours post treatment (4 hpt). (**F**) Species-specific differences in *Cd302* evolution. Left: Phylogenetic tree depicting the evolutionary relationships of placental mammal *Cd302* sequences with significant bootstrap values (>70%) displayed below the corresponding branches. The basal lineage leading to mice/rats is highlighted in red. The marsupial *Cd302* sequence from the Tasmanian devil was used as an outgroup. Right: Protein cartoon denotes the relative functional domains of mCd302 with the position of coding mutations unique to the rat/mouse specific lineage highlighted below.

confocal microscopy, with distribution throughout the cytosol and a notable fraction of mCr1l localized to a perinuclear compartment (Fig. 4B). In situ staining of formalin fixed paraffin embedded (FFPE) mouse liver slices confirmed mCr1l membranous localization in hepatocytes (Fig. 4C) and, in agreement with this observation, flow cytometry of nonpermeabilized mouse hepatocytes revealed a subfraction of both proteins localized to the cell surface (Fig. 4D). Together, these data confirm constitutive expression of *mCd302* and *mCr1l* mRNAs and encoded protein in murine livers and hepatocytes, the analogous target cells for HCV infection in humans.

Antiviral responses to RNA viruses in hepatocytes are mediated by at least two distinct, non-overlapping sensing pathways: retinoic

acid inducible gene I (RIG-I) and Toll-like receptor 3 (TLR3) (*23*). To determine whether *mCd302* or *mCr1l* expression is modulated by either pathway, we treated murine primary hepatocytes with either IFNα2a or the double-stranded RNA mimic polyinosinic:polycytidyl acid (polyI:C). Compared to control IRGs, we did not detect dysregulation of *mCd302* or *mCr1l* mRNAs, indicating that their expression is constitutive and regulated by neither RIG-I nor TLR3 sensing pathways (Fig. 4E).

The human and rodent lineages diverged 80 to 90 million years ago (*24*), and infection of immunocompetent mice with HCV is not possible. The *Cd302* gene is conserved throughout mammalian evolution, and phylogenetic analysis of *Cd302* coding sequences from representative mammalian species revealed reconstruction of the superordinal groupings predicted using multikilobase genomic loci (*24*). However, inconsistent with the organismal phylogeny, the positioning of the rat/mouse orthologs with other rodent species (guinea pig) was not supported, with these two species located antecedent to the placental grouping (Fig. 4F, left). This basal positioning of rat/mouse orthologs was supported by significant bootstrap values. Closer inspection revealed fixation of nine unique nonsynonymous mutations on the rat-mouse lineage, distributed throughout the protein but concentrated in cytoplasmic tail (Fig. 4F, right). Together, these data indicate a unique evolutionary trajectory for rat/murine *Cd302*, with the fixation of multiple mutations on the rat:mouse branch giving rise to the incongruence between organismal and *Cd302* phylogenies. This likely represents the signature of selection in response to pressure from pathogens and/or the possible acquisition of a novel biological function (e.g., antiviral restriction) or interaction partner (e.g., m*Cr1l*). Phylogenetic analysis of mammalian *Cr1l* was not possible due to high levels of sequence divergence including indels (see Fig. 5B), coupled with the absence of a *Cr1l* ortholog in many mammal species.

Human hepatocytes lack *CR1L* mRNA expression but express *CD302*, limiting HCV infection

To explore whether *CD302* and/or *CR1L* may have broader relevance for HCV permissiveness in humans, we aligned the human and murine protein orthologs of both factors. The hCD302:mCd302 alignment revealed ~75% amino acid conservation, with hydrophobicity plotting identifying putative conserved transmembrane domains, implying membrane incorporation in both species (Fig. 5A). Differences between human and mouse were concentrated in the cytoplasmic tail domain. In contrast, hCR1L:mCr1l proteins shared only ~35% sequence identity, with large differences observed in the size of the translated protein. Hydrophobicity plotting identified a putative transmembrane region in murine Cr1l, although this domain was absent in human CR1L (Fig. 5B).

To investigate whether mRNA transcript abundance in hepatocytes is conserved between mice and humans, we conducted transcriptomic profiling of plated PHHs from multiple donors. While *hCD302* transcripts were readily detected at similar levels to that observed in mice, *hCR1L* transcripts were virtually undetectable or completely absent, comparable to brain- or lung-specific mRNAs (Fig. 5C). Together, these data confirm constitutive expression of *hCD302* mRNA in PHHs but the absence of *hCR1L*, suggesting that the combined potent and cooperative anti-HCV restriction provided by coexpression of both factors in mice is absent in the human liver. To test the human orthologs' ability to restrict HCV infection, we ectopically expressed *hCD302* and *hCR1L* in Huh-7.5 cells followed by infection with R-luc reporter HCV. Comparable to *mCd302*, we observed a potent reduction of intracellular RLU accumulation over a 4- to 96-hour time course for *hCD302* (Fig. 5D). However, *hCR1L* mediated no effect on the ability of HCV to infect hepatoma cells. To determine whether expression of *hCD302* in PHHs is modulated by the RIG-I or TLR3 sensing pathway, we treated PHHs with either IFNα2a or polyI:C. Similar to mouse hepatocytes, we did not detect a dysregulation of *hCD302* mRNA when compared to control genes, indicating that its expression is steady state and not regulated by either the RIG-I or TLR3 sensing pathways (Fig. 5E). The inability of the human ortholog of *CR1L* to restrict HCV, combined with an absence of *CR1L* mRNA in PHHs, highlights the differences between human and mouse with respect to intrinsic liver defenses: The combined cooperative antiviral restriction provided by both factors is absent in humans. Nonetheless, h*CD302* alone was able to restrict HCV infection, which warrants further investigation.

C-type lectins make up a large superfamily of proteins with diverse functions. A unifying feature of this group of proteins is the CTLD fold, which is characterized by a double-loop structure that is stabilized by conserved disulfide bridges at the bases of these loops. The presence or absence of the so-called long loop region is used to divide CTLDs in two groups: Classical CTLDs (e.g., dendritic cell-specific intercellular adhesion molecule-3-grabbing non-integrin: DC-SIGN) have a long loop region, which is absent in the more compact CTLDs (e.g., human CD44). The long loop region is involved in Ca^{2+}-dependent carbohydrate binding and also in the binding of other ligands (*25*). Recently, the nuclear magnetic resonance (NMR) structure of the hCD302 extracellular domain was solved, showing that it comprises a canonical CTLD fold with a long loop region (Fig. 5F, right) (*26*). Superposition of an mCd302 CTLD homology model onto the CTLD structure of hCD302 revealed a large number of surface residues conserved between mouse and human CTLDs (Fig. 5F, left). This finding suggests conservation of ligand specificity between the mouse and human orthologs. In contrast, alignment of CPT regions highlights differences between human and mouse and may point to potential differences in downstream signaling between the species (Fig. 5F, bottom).

Enhanced murine hepatocyte susceptibility to an adapted HCV population

The minimal requirements for HCV entry into murine hepatocytes are the ectopic expression of human entry factors *OCLN* and *CD81* (*12*). Consequently, we generated humanized hOC^{hep} mice, which conditionally express human *CD81* and *OCLN* in hepatocytes ($hOCLN^{+/-}$ $hCD81^{+/-}$). To examine the relevance of endogenous *Cd302* and *Cr1l* expression for HCV restriction, we explored whether knockdown of *mCd302* and *mCr1l* in plated primary hOC^{hep} cells modulated the cellular response to infection and increased HCV permissiveness. To this end, we silenced *mCd302* and *mCr1l* mRNA in plated hOC^{hep}, followed by HCV infection (strain Jc1) and transcriptional profiling. The antiviral response to HCV infection was greater in plated hOC^{hep} previously treated with *mCd302* and *mCr1l* targeting small interfering RNAs (siRNAs) when compared to hepatocytes transfected with control siRNAs (Fig. 6A). We did not observe this trend in PMH from a WT mouse lacking the human entry factors, indicating an HCV entry–associated process. These data suggested that *mCd302* and *mCr1l* silencing facilitates more efficient HCV entry into murine hepatocytes, resulting in a concomitant increase in the magnitude of the murine hepatocyte antiviral response. However, we did not observe subsequent viral replication

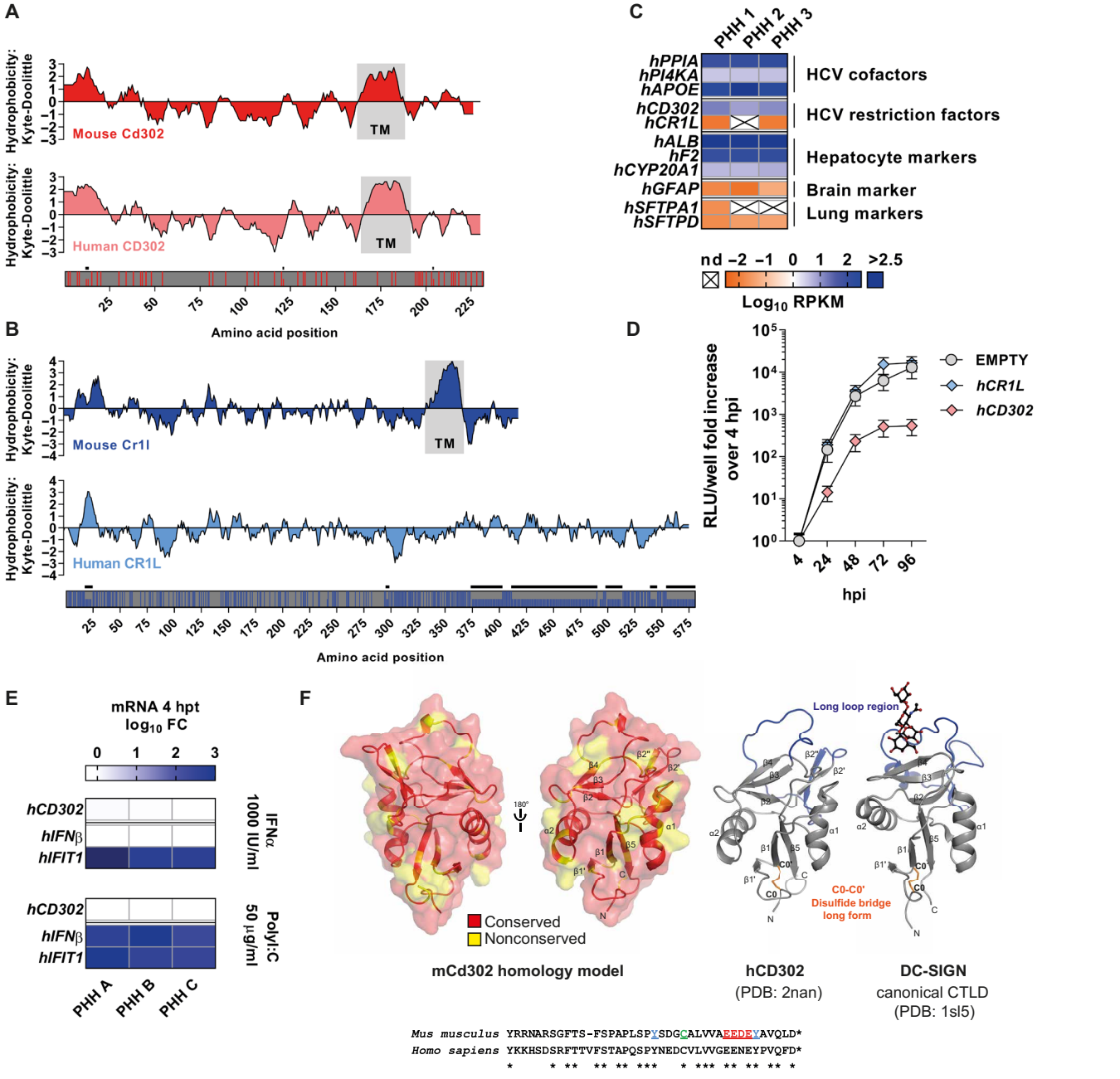

Fig. 5. Human-mouse differences in HCV restriction and hepatocyte expression. (**A**) Human CD302 and mouse Cd302 are transmembrane proteins. Hydrophobicity plotting reveals putative TM domains highlighted in gray. Highlighter plots positioned below visualize amino acid conservation between the species. Colored bars represent amino acid changes in the human homolog relative to the mouse protein sequence, while gray bars represent conserved residues. Black bars located above highlighter plot indicate indels. (**B**) Mouse Cr1l is a transmembrane protein, but human CR1L is not. (**C**) Human hepatocytes lack intrinsic h*CR1L* mRNA expression. Intrinsic mRNA expression of selected genes in PHHs from $n = 3$ donors. Cells with X represent genes with no detectable expression (RPKM = 0). (**D**) Human *CD302* and restricts reporter HCV infection but human *CR1L* does not. HCV infection of Huh-7.5 cells overexpressing the indicated genes. Curves represent fold RLU increase over 4 hpi, and values presented are means of $n = 5$ experiments ± SEM. (**E**) Human *CD302* mRNA is not inducible. Heatmaps showing fold change in mRNA expression of candidate genes in PHHs from $n = 3$ donors, which were either untreated or treated with IFNα2a or Poly:C. Fold regulation was compared to *IFNβ* or *IFIT1* induction. (**F**) Extracellular domain homology model for mCd302. Left: Homology model based on the NMR structure of hCD302 (PDB 2NAN) is shown in cartoon surface representations with nonconserved residues highlighted in yellow. Right: Structural comparison of hCD302 with the canonical CTLD of DC-SIGN according to the classification of (*25*). Both proteins are shown in cartoon representation with the cysteine bridge specific for long-form CTLDs highlighted as orange sticks. The oligosaccharide LNFPIII bond to DC-SIGN in the representative DC-SIGN-glycan complex structure (PDB 1SL5) is shown in ball-and-stick representation. Amino acid alignment of the human-mouse cytoplasmic tail region is positioned below.

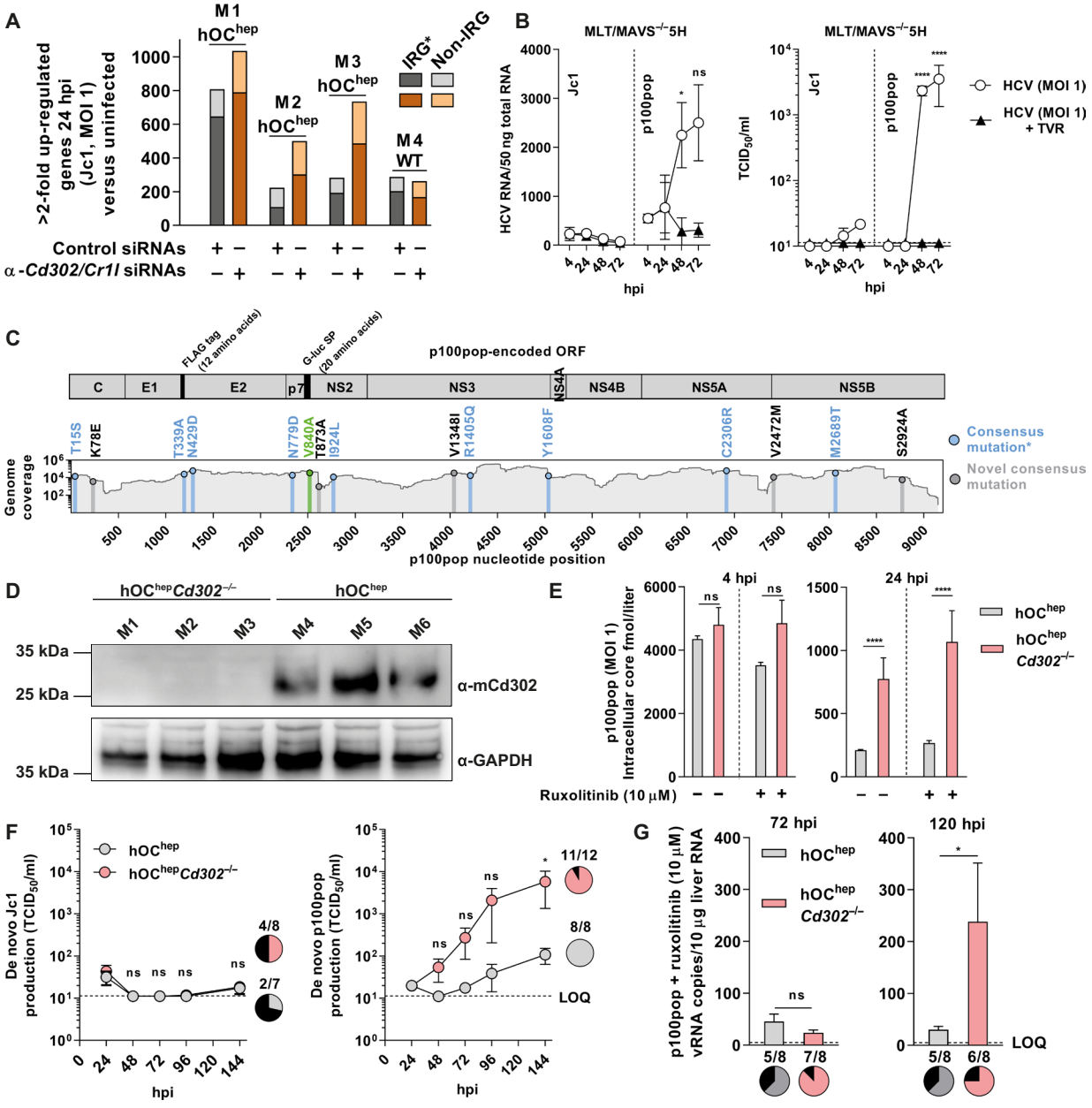

Fig. 6. Ablation of endogenous *Cd302* expression in humanized murine hepatocytes enhances HCV permissiveness. (**A**) Silencing endogenous *mCd302*/*mCr1l* expression increases HCV uptake. Hepatocytes were transfected with the indicated siRNAs, followed 24 hours later by HCV infection. Numbers of genes >2-fold up-regulated were quantified at 24 hpi by comparison with uninfected hepatocyte transcriptomes transfected with the corresponding siRNAs. *IRGs determined using (*22*). (**B**) HCV strain p100pop exhibits enhanced replication in murine cells. MLT-MAVS$^{-/-}$5H cells were infected with the indicated HCV strains. Intracellular vRNA and virion production were monitored, and data represent the means of $n = 3$ experiments ± SEM. Telaprevir (TVR). (**C**) Consensus mutations in the p100pop genome relative to parental Jc1. Data represent next-generation sequencing (NGS) coverage across the genome with nonsynonymous mutations detectable at a population frequency >50% highlighted. *Blue mutations are described in (*27*), gray mutations represent novel mutations identified by NGS, and the single green mutation was detected in the retained G-luc SP. (**D**) CRISPR-Cas9 ablation of endogenous *Cd302* expression. GAPDH, glyceraldehyde-3-phosphate dehydrogenase. Western blot comparison of Cd302 protein expression in plated hepatocytes from the indicated mice. (**E**) Endogenous *Cd302* knockout increases HCV uptake. Hepatocytes from the indicated mice were infected with p100pop, with and without ruxolitinib treatment. Intracellular core was determined after extensive PBS washing. Data represent means + SEM for $n = 3$ experiments. (**F**) Endogenous *Cd302* knockout increases de novo HCV production. Hepatocytes from the indicated mice were pretreated with ruxolitinib, infected with either Jc1 or p100pop, and virion production monitored. Data represent mean values ± SEM from productive infections, which are presented as associated pie charts. Black, no infection; gray or pink, productive infection. (**G**) *Cd302* knockout in improves intrahepatic HCV replication. Quantification of intrahepatic p100pop vRNA after intrasplenic inoculation. Data represent mean values + SEM from productive infections, which are presented as associated pie charts. ****$P < 0.0001$ and *$P < 0.05$.

in plated hOC^{hep}. In contrast, siRNA targeting of ectopically expressed *mCd302*, *mCr1l*, or *mCd302* and *mCr1l* in Huh-7.5 cells increased Jc1 replication (fig. S5). To overcome the observed block on HCV replication in murine hepatocytes, we compared fitness of parental HCV (strain Jc1) with an HCV population derived from Jc1 after 100 passages (p100pop) in Huh-7.5 cells, which exhibits enhanced replicative fitness and partial resistance to IFN (*27*). Infection of mouse liver tumor (MLT) cells that ectopically express five human factors (*CD81*, *SCARB1*, *CLDN1*, *OCLN*, and *APOE*: 5H) coupled with blunted innate immune signaling due to ablation of mitochondrial antiviral-signaling protein (MAVS) expression (MLT/MAVS$^{-/-}$5H) (*10*) revealed significantly enhanced permissiveness to p100pop when compared to parental Jc1 (Fig. 6B). Suppression of p100pop replication in MLT/MAVS$^{-/-}$5H was also demonstrated using teleprevir, an HCV NS3 protease inhibitor (Fig. 6B). This enhanced replicative fitness was correlated with 14 nonsynonymous mutations with >50% population frequency distributed throughout the p100pop open reading frame (ORF) (Fig. 6C). Although p100pop exhibits enhanced replicative capacity in murine liver cells, this strain was susceptible to *mCd302*/*mCr1l* restriction, albeit to a lesser extent than parental Jc1 (fig. S6).

Cd302 knockout modulates the murine hepatocyte transcriptome and increases HCV permissiveness

Silencing of *mCd302* and *mCr1l* was effective in humanized mouse hepatocytes, leading to increased HCV uptake and a concomitant increase in innate cellular responses (Fig. 6A). However, because of high intrinsic expression, targeted mRNAs encoding functional *mCd302* and *mCr1l* were still detected. To overcome this limitation, we deleted Exon 1 of the *mCd302* locus in hOC^{hep} mice using CRISPR-Cas9 technology. Comparative Western blotting of primary hepatocytes from hOC^{hep} and hOC^{hep} *Cd302*$^{-/-}$ mice revealed complete ablation of functional Cd302 protein expression (Fig. 6D). Unfortunately, *mCr1l*$^{-/-}$ knockout mice were not viable due to an embryonically lethal phenotype (*28*). To determine whether *mCd302* deletion modulated the intrinsic murine hepatocyte transcriptome, we performed global RNA-seq profiling on primary hepatocytes isolated from hOC^{hep} and hOC^{hep} *Cd302*$^{-/-}$ mice. These analyses revealed 289 significant DEGs in hepatocytes from hOC^{hep} *Cd302*$^{-/-}$ mice when compared to control hOC^{hep} mice, confirming a role for *mCd302* in the regulation of constitutive gene expression levels in murine hepatocytes. Gene Ontology (GO) analyses revealed significant and overlapping dysregulation of genes associated with cellular defense and the inflammatory response, in addition to modulation of gene expression associated with hepatocyte metabolic processing (fig. S7, left). Analogous to overexpression of mouse *Cd302*/*Cr1l* in human cell lines where antiviral genes were generally up-regulated, ablation of endogenous *Cd302* expression in mouse hepatocytes resulted in down-regulation of a subset of genes involved in virus defense and the inflammatory response (e.g., *Apobec1*, *Isg20, Oasl1*, *Ccl7*, and *Cxcl9*) (fig. S7, top right). In addition, dysregulation of genes associated with metabolic processing of lipids and fatty acids was also affected (e.g., *Fabp4*, *Fabp5*, and *Plin5*) (fig. S7, bottom right). A total of 159 of 289 DEGs were classified as IRGs.

To determine the effect of endogenous *Cd302* knockout on HCV permissiveness, we infected either plated primary hepatocytes isolated from hOC^{hep} or hOC^{hep} *Cd302*$^{-/-}$ mice with p100pop, blunting IFN responses with ruxolitinib. At 4 hpi, we detected higher levels of cell-associated HCV core protein in hOC^{hep} *Cd302*$^{-/-}$ hepatocytes when compared to hOC^{hep} controls (Fig. 6E, left). Cell-associated HCV core protein was reduced at 24 hpi likely due to vigorous IFN-dependent antiviral defenses. However, a significant difference was apparent between hepatocytes isolated from hOC^{hep} *Cd302*$^{-/-}$ and hOC^{hep} mice, with two- to fourfold greater cell-associated core detected, which could be further enhanced by JAK/STAT inhibition (Fig. 6E, right). These data suggested that ablation of endogenous *Cd302* expression in humanized mouse hepatocytes increased infection by human-tropic HCV. Building on these data, we performed a time course comparison, infecting hepatocytes isolated from both hOC^{hep} and hOC^{hep} *Cd302*$^{-/-}$ mice with either Jc1 or p100pop after JAK/STAT inhibition, and monitored de novo virus production at 24 to 144 hpi. No differences in virion release were observed between hepatocytes from hOC^{hep} and hOC^{hep} *Cd302*$^{-/-}$ mice infected with Jc1, with limited de novo HCV production detected (Fig. 6F, left). In contrast and despite differences observed between individual animals, de novo p100pop production was demonstrably increased in hepatocytes isolated from hOC^{hep} *Cd302*$^{-/-}$ mice when compared to parallel control hepatocytes from hOC^{hep} mice at 48 to 144 hpi, with up to 50-fold greater mean virus production observed (Fig. 6F, right). To investigate whether this observation could be replicated in vivo, we performed intrasplenic inoculation of hOC^{hep} or hOC^{hep} *Cd302*$^{-/-}$ mice with p100pop, with continued oral administration of ruxolitinib to suppress antiviral defenses mediated by JAK/STAT signaling (Fig. 6G). Serum and liver vRNA were assessed at 72 and 120 hpi. No differences were observed in serum vRNA between hOC^{hep} and hOC^{hep} *Cd302*$^{-/-}$ mice at either time point, indicating a potential block on virus release in the murine liver. In contrast, at 120 hpi, mean liver-resident vRNA was ca. 7-fold higher in hOC^{hep} *Cd302*$^{-/-}$ mice compared to hOC^{hep} animals, and only hOC^{hep} *Cd302*$^{-/-}$ mice displayed a significant increase of liver-resident virus load from 72 to 120 hpi (Fig. 6G). In summary, these data confirm that *Cd302* contributes to the species barrier limiting HCV infection of murine hepatocytes, both in vivo and ex vivo.

DISCUSSION

The tolerogenic environment of the liver represents an attractive replication environment for pathogens enabling the establishment of chronic infection by HCV. Using cDNA library screening, we identified a lectin and a complement receptor, Cd302 and Cr1l, as previously unreported species barrier determinants contributing to HCV restriction in the murine liver. Our data demonstrate that *mCd302* and *mCr1l* expression is constitutive in murine hepatocytes and not inducible by IFN: These factors mediate protection independently of the IFN system. We observed differences in liver expression and the ability to restrict HCV between the murine orthologs and their human counterparts. The unique evolutionary trajectory of mouse:rat *Cd302*, which is largely due to differences concentrated in the short cytoplasmic tail, coupled with the lack of an interaction partner (Cr1l) to amplify any potential signal in humans, suggests that murine Cd302 has acquired a unique or enhanced antiviral function when compared to its human ortholog. Rodents (similar to bats) have high population densities in the wild and consequently represent reservoirs for many pathogens. Therefore, it is possible that mice might have evolved novel or enhanced antiviral strategies to cope with these more frequent pathogen exposures when compared to humans. Despite the differences observed between humans and mice, human *CD302* mRNA was also abundant in PHHs, and ectopic expression of

human *CD302* in hepatoma cells mediated an anti-HCV phenotype. Although outside the scope of this investigation, determining whether different allelic variants or differing *hCD302* expression levels in the livers of HCV-infected patients is correlated with disease outcome (e.g., severity of liver disease or viral clearance versus persistence) is currently the subject of further investigation.

Mechanistically, our data support a model where the murine transmembrane proteins Cd302 and Cr1l interact with each other and with virions to impede HCV cell entry. Competition with virus binding to canonical entry factors may impede virus trafficking to tight junctions and, in turn, productive infection. In addition, ectopic expression of murine factors in human hepatoma cells resulted in the cooperative induction of a noncanonical transcriptional program. Moreover, modulation of the intrinsic murine hepatocyte transcriptome was observed upon Cas9 disruption of endogenous *Cd302* expression. To further dissect these observations, we used ingenuity pathway analysis (IPA) to compare gene expression changes observed between Huh-7.5 and Huh-7.5 [*mCd302*/*mCr1l*] cells with those observed between humanized hOC^{hep} and hOC^{hep} $Cd302^{-/-}$ PMHs. Modulation of *mCd302* expression targeted common pathways in human and mouse liver cells: 16 significantly enriched canonical pathways were shared between both systems including four pathways associated with related nuclear receptors (NRs) (fig. S8A). NRs are known to regulate transcriptional programs that control host metabolic processes including lipid metabolism. In addition, NRs have been implicated in host-virus interactions, modulating susceptibility to both DNA and RNA virus infections (*29*). NRs have been shown to control both pro- and antiviral metabolic responses to HCV in PHHs (*30*). The top hit in both the human and mouse systems represents an NR pathway "LPS/IL-1 mediated inhibition of retinoid X receptor (RXR) function" that influences downstream lipid and fatty acid metabolism. Detailed inspection of shared NR pathways identified significantly dysregulated molecules at multiple pathway stages and contained shared and distinct molecules in both systems (fig. S8B). Corresponding changes in gene expression for targeted pathways in both systems highlights opposing transcriptional dysregulation of gene subsets in these analogous in vitro and ex vivo systems (fig. S8C). Thus, in both human overexpression and in mouse knockout systems, gain or loss of *Cd302* expression influences RXRα NR signaling: RXRα-dependent genes and their roles in lipid and fatty acid metabolism likely contribute to the resulting antiviral state, as the HCV life cycle is tightly coupled to lipid and fatty acid metabolism.

Cas9 disruption of *Cd302* expression in murine hepatocytes, humanized for productive HCV entry, increased permissiveness for an adapted HCV population both ex vivo and in vivo. We demonstrate that p100pop, an HCV population that developed enhanced replication fitness and partial IFN resistance in human cells, also exhibits enhanced fitness in humanized mouse liver cell lines and in humanized PMHs when compared to its parent virus. The enhancement of HCV permissiveness mediated by ablation of *Cd302* liver expression in mice was only detectable when infection experiments were performed using p100pop, pointing to additional uncharacterized barriers to efficient HCV propagation in the murine liver. These barriers could represent missing or incompatible human cofactors—or additional murine restriction factors targeting HCV. It is likely that the enhanced replication fitness and reduced IFN sensitivity of p100pop enables a partial overcoming of these additional replication blocks that is not achieved by nonadapted strains. Therefore, p100pop represents a good starting point for development of more robust HCV mouse models, and stepwise adaptation of HCV to complete its full replication cycle in murine hepatocytes may also be possible. However, for the purposes of HCV vaccine development, these adapted viruses should retain the key attributes of strains that infect humans, e.g., receptor usage and immunogenicity.

The murine *Cd302* gene is expressed in various myeloid cell types and different murine tissues, most prominently in the liver (*20*, *21*). While a role in regulating myeloid cell migration was previously reported, the functional importance of hepatocyte-expressed *mCd302* remained elusive until now. Lectins expressed in myeloid cells play important roles in immune defenses (*31*). They recognize pathogens via their CTLDs and trigger responses such as endocytosis, phagocytosis, and release of pro- or anti-inflammatory cytokines. Moreover, the complement system is essential for pathogen clearance. Here, we report an unexpected cooperation between a hepatocyte-expressed lectin and a complement receptor in mice. This work highlights convergence of lectin and complement systems for shaping liver intrinsic immunity and draws attention to a complex antiviral mechanism involving entry inhibition and metabolic reprogramming. Combining humanization of murine hepatocytes with ablation of a constitutively expressed antiviral defense system—the *mCd302*/*mCr1l* axis—and using an adapted HCV population with enhanced replication capacity in murine cells opens new avenues for the development of more robust HCV mouse models. Such a model will be of high value for development and safety testing of prophylactic vaccines to complement existing therapies for global control of and ultimate eradication of the HCV disease burden.

MATERIALS AND METHODS

Library generation, delivery, and screening

To generate a Mouse IFNα-Induced Liver Library (MIILL), a single mouse was injected with IFNα and euthanized at 4 hours post IFN induction. The liver was homogenized in TRIzol reagent (Invitrogen), and total RNA was extracted. The $PolyA^+$ component of the total RNA was enriched using an Oligotex mRNA kit (QIAGEN). Using components from a SMART cDNA Library Construction Kit (Clontech), mRNA was reverse-transcribed into cDNA and size-fractionated before ligation into the lentiviral vector pV1. Ligated fractions were electroporated into ElectroMAX DH5α (Invitrogen) cells according to the manufacturer's specifications, and resulting colonies were sequenced to ascertain the library quality. Ligated fractions that contained high percentages of diverse full-length mouse ORFs were pooled and electroporated before solid phase amplification in approximately 8 liters of medium. Before solid phase amplification, the MIILL contained 4×10^6 independent clones. After solid phase amplification, the pV1 MIILL was extracted from transformed bacteria using a Maxiprep protocol (Macherey Nagel), aliquoted, and stored at −20°C. The library was packaged into VSV-G–enveloped psuedoparticles via three-plasmid transfection into 293T cells. VSV-G, HIV-1gag/pol, and pV1 MIILL plasmids were transfected in equimolar amounts using Lipofectamine 2000 (Invitrogen), and supernatants were harvested at 24 and 48 hours after sodium butyrate induction. Titers of MIILLpps were calculated via median tissue culture infectious dose ($TCID_{50}$) limiting dilution onto HeLa-TZMbl cells. Cells were fixed and stained 72 hpi, and MIILLpps were aliquoted and stored at −80°C. Permissiveness of different cell lines for MIILLpp transduction was determined via fluorescence-activated cell sorting

(FACS) using pV1 green fluorescent protein–containing pseudoparticles. We delivered our MIILL (one to two particles per cell) to highly permissive n4mBid hepatoma cells. These cells are modified Huh-7.5 cells, which undergo programmed cell death upon HCV replication (*13*). Iterative rounds of selection were performed with WT HCV [Jc1: multiplicity of infection (MOI) 50], and surviving cells were expanded. Permissiveness to HCV/coronavirus (CoV) infection was assessed using R-luc reporter viruses.

RNA-seq

Total RNA from primary cells and cell lines was extracted using a NucleoSpin RNA kit (Macherey Nagel) or TRIzol reagent (Invitrogen) according to the manufacturer's instructions. RNA quality checking was performed using an Agilent Bioanalyzer, and sequencing libraries were generated using a ScriptSeqv2 kit (Illumina) according to the manufacturer's instructions. RNA-seq was performed using the Illumina HiSeq 2500 or NovaSeq platforms. Transcriptomic analyses were performed using CLC Genomics Workbench (QIAGEN). Raw FASTQ files were mapped against the hg19 human or mm9 *Mus musculus* reference genomes with annotated gene and mRNA tracks. Gene expression was calculated for individual transcripts as RPKM, and identification of DEGs was performed. GO analyses were conducted using the GO resource (http://geneontology.org/). Significantly enriched GO categories were identified using the PANTHER Classification system (http://pantherdb.org/). *P* values for GO categories were adjusted for multiple testing using the Bonferroni correction.

vRNA isolation, NGS library preparation, and Illumina sequencing of HCV p100pop

Isolated vRNA was used for Illumina library preparation using a modified protocol of the NNSR priming method (*32*). Briefly, for the RT, 5 μl of RNA and 100 pmol NNSR_RT primer (gctcttccgatctct-NNNNNN) were heat denatured at 65°C for 5 min and chilled on ice. The reactions were supplemented with first-strand synthesis buffer, 10 mM dithiothreitol, 0.05 mM deoxynucleotide triphosphates (dNTPs), 20 units of RiboLock ribonuclease (RNase) inhibitor, and 200 units of Superscript III reverse transcriptase (Thermo Fisher Scientific). Volumes were standardized to 20 μl, and reactions were incubated at 45°C for 30 min followed by heat inactivation at 70°C for 15 min. The nucleic acids were purified with magnetic beads, and the RNA was digested with RNase H [New England Biolabs (NEB)] for 20 min at 37°C. After bead purification, cDNA samples were subjected to second-strand synthesis at 37°C for 30 min in a 50-μl final reaction volume containing the following: NEB buffer 2, 0.125 mM dNTPs, 5 units of 3′-5′exo-Klenow Fragment (NEB), and 200 pmol NNSR-2 primer (gctcttccgatctgaNNNNNN). After magnetic bead purification, the double-stranded cDNA served as the template for PCR amplification to obtain the barcoded Illumina libraries. The PCRs were performed using the NEBNext Ultra II Master Mix (NEB) containing 25 pmol NNSRnest_ind_N (caagcagaagacggcatacgagat-NNNNNNgtgactggagttcagacgtgtgctcttccgatctga) and NNSR_Illumina (aatgatacggcgaccaccgagatctacactctttccctacacgacgctcttccgatctct) primers, each using the following cycling conditions: 98°C for 10 s; 5 cycles of 98°C for 10 s, 55°C for 30 s, and 68°C for 30 s; and 15 cycles of 98°C for 10 s, 65°C for 30 s, and 68°C for 30 s. The resulting 300- to 700–base pair (bp) DNA smears were isolated from 1.5% agarose gels with the Zymoclean Gel DNA Recovery Kit (Zymo Research), quantified with qPCR using the NEBNext Library Quant Kit for Illumina (NEB), and sequenced on a MiSeq instrument with a paired-end 2 × 300 setting.

Stable cell line generation

For ectopic expression of human or murine genes, gBlock gene fragments were ordered (Integrated DNA Technologies) and cloned into the lentiviral vector pWPI (Addgene) via restriction cloning (encoding either blasticidin or puromycin resistance genes). Correct orientation and nucleotide sequences of inserts were verified by Sanger sequencing (GATC). Lentiviral plasmids were packaged into VSV-G–enveloped pseudoparticles via three-plasmid transfection into 293T cells. VSV-G, HIV-1gag/pol, and pWPI plasmids were transfected in equimolar amounts using Lipofectamine 2000 (Invitrogen), and supernatants were harvested at 24 and 48 hours after sodium butyrate induction. Pooled supernatants were filtered (45-μm pores) and used to transduce 2×10^5 Huh-7.5 cells. Seventy-two hours after transduction, selection markers were added to media, and surviving cells were expanded.

Cell lines

All cancer cell lines were cultured in Dulbecco's modified Eagle's medium (DMEM) (Invitrogen) supplemented with nonessential amino acids (Invitrogen), 2 mM L-glutamine (Invitrogen), and 10% fetal calf serum (FCS) (PAA Laboratories GmbH). For selection of lentiviral transduced cell lines, blasticidin (5 μg/ml; Invivogen) or puromycin (2 μg/ml; Sigma-Aldrich) was added. To induce polarization, cells were trypsinized and resuspended in DMEM + 10% fetal bovine serum (FBS) for a final concentration of 1×10^5 cells/ml. Thawed Matrigel (Growth Factor Reduced, Phenol Red-free; Sigma-Aldrich) and cells were combined in equal parts, seeded onto coverslips in 24-well plates (75 μl per well), and then incubated at 37°C until polymerized. DMEM + 10% FBS was added to each well, and cells were cultured for 7 days, changing the media every other day.

Viruses

WT, p100pop (provided as a gift from E. Domingo, Madrid, Spain), and R-luc and F-luc reporter HCV viruses were produced as previously described. Human CoV 229E R-luc reporter virus was provided as a gift from V. Theil (Bern, Switzerland). For DiD labeling, HCV stocks were concentrated using PEG (polyethylene glycol 8000; Thermo Fisher Scientific) precipitation resuspended in serum-free media and then labeled with 5 μl of DiD (Invitrogen) per 1-ml concentrated virus for 90 min. The virus was then added to a 10 to 60% weight/volume iodixanol gradient (OptiPrep, Sigma-Aldrich) and centrifuged for 16.5 hours at 34,000 rpm (4°C). The resulting gradient was separated into 1-ml fractions; each was assayed for specific infectivity (*33*). Fractions with acceptable specific infectivity (<10) were purified via Amicon Ultra 100K filters (Millipore).

Huh-7.5 cells stably expressing *SEC14L2* and murine restriction factors were infected with serum from acute-phase or post-transplant patients with HCV as previously described (*15*). Briefly, cells were seeded into 24-well plates at a density of 50,000 cells per well and grown overnight. The cells were then infected with 25 μl of patient serum diluted in 500 μl of DMEM containing 10% FBS, 1× non-essential amino acids (NEAA), and epidermal growth factor (EGF; 50 ng/ml). After overnight incubation with serum, cells were rinsed twice with 1× phosphate-buffered saline (PBS) and fed with 500 μl of fresh medium containing 10% FBS, 1× NEAA, and EGF (50 ng/ml). Two days later, the cells were transferred to the 12-well plates and grown for another 3 days before they were harvested for RT-qPCR.

HEV constructs based on the genotype 3 Kernow C1 strain p6, S10-3 cells, and anti-ORF2 antibody were a gift from S. Emerson,

National Institutes of Health. To prepare the vRNA for transfection, HEV plasmids p6, p6Gluc, and p6Gluc/GAD active site mutant (*34*) were linearized with the restriction enzyme Mlu I, and in vitro transcription was performed using the mMESSAGE mMACHINE Kit (Life Technologies). Two hundred nanograms of in vitro–transcribed vRNA was transfected into 1×10^5 S10-3 cells per well of a 12-well cell culture plate using the TransIT-mRNA transfection kit (Mirus Bio LLC, Madison, WI). For cells transfected with the subgenomic replicon p6GLuc ± GAD, medium was changed every 24 hours and harvested for GLuc quantification. Full-length virus p6 was harvested as previously described (*35*). HEV focus-forming units were quantified by staining for anti-HEV capsid ORF2.

Huh-7.5 cells stably expressing murine restriction factors were infected with DENV (16681 strain) (MOI 0.5), YFV 17D vaccine strain, the parental Asibi strain (MOI 1), and WNV (lineage 1 strain, WNV-TX02) (MOI 0.5). Cells were stained for flow cytometry using the following: rabbit polyclonal anti-NS3 antibody (GeneTex, cat. no. GTX124252, 1:500) for DENV, mouse monoclonal antibody (Santa Cruz Biotechnology, cat. no. SC58083, 1:500) for YFV, and mouse monoclonal anti-NS1 antibody (BEI Resources, cat. no. 10145, 1:500) for WNV.

For RSV F-luc virus production, Hep2 cells (American Type Culture Collection CCL-23) were grown in advanced MEM medium (Thermo Fisher Scientific, Waltham, MA) supplemented with 10% heat-inactivated FCS (Capricorn Scientific, Ebsdorfergrund, Germany), 2 mM L-glutamine (Thermo Fisher Scientific, Waltham, MA), penicillin and streptomycin (100 U/ml; Thermo Fisher Scientific, Waltham, MA), and 1× nonessential amino acids (Thermo Fisher Scientific, Waltham, MA) at 37°C in humidified air with 5% CO_2. HEp2 cells were seeded in 15-cm cell culture dishes (Corning Incorporated, Life Sciences, Oneonta, NY) to reach 60 to 70% confluence the next day. Twenty-four hours later, medium was removed, and 5 ml of FCS-free advanced minimal essential media (adv. MEM) containing 4×10^5 $TCID_{50}$/ml of recombinant human respiratory syncytial virus (HRSV) subtype A F-luc reporter virus (provided by J.-F. Éléöuet) was added. Cells were incubated at 37°C and gently shaken for 4 hours. Medium was replaced with adv. MEM containing 2% FCS followed by further incubation at 37°C until syncytia formation was prominent. Supernatant and cells were harvested, supplemented with 10% of virus stabilizer buffer [1 M $MgSO_4$ and 0.5 M Hepes (pH 7,5)], and vortexed vigorously for 2 min to release cell-attached virus particles. Debris was removed by centrifugation at 1000*g* for 5 min, and cell-free supernatant was frozen in −80°C cold ethanol for 12 hours and then transferred to long-term storage at −80°C.

Isolation of primary hepatocytes

Hepatocytes were isolated from mice by a modified two-step Liberase perfusion (*36*). Briefly, mice were anesthetized using Ketamine (Albrecht) and Rompun (Bayer). The body cavity was opened, and a catheter was placed into the portal vein and connected to a flow pump, which pumped media prewarmed at 37°C from a water bath into the catheter, and the vena cava was cut. The liver was first perfused with Earle's balanced salt solution (EBSS) (Gibco) solution containing 0.5 mM EGTA (Sigma-Aldrich) and 10 mM Hepes buffer (Sigma-Aldrich). Subsequently, EBSS supplemented with 10 mM Hepes buffer and Liberase (100 μg/ml; Roche) was applied for enzymatic digestion of the tissue at 37°C. After digestion for 10 to 12 min, the liver was carefully disconnected and tissue was manually disrupted with sterile scissors and scalpel in DMEM (Gibco) containing 10% FCS (PAN-Biotech). The suspended hepatocytes were passed through a 100-μm nylon filter into 50-ml Falcon tubes. The cell suspensions were centrifuged twice at 300 rpm for 5 min at 4°C, and cell pellets were resuspended in ice-cold DMEM containing 10% FCS. Cell viability was tested by trypan blue (Fluka) before plating on collagen-coated six-well dishes. Approximately 5×10^5 cells were plated per well, and supplemented hepatocyte culture media (HCM) (Lonza) were used to maintain primary hepatocytes in culture.

Plated PHHs were obtained from the Department of General, Visceral, and Transplant surgery at Hannover Medical School and cultured as previously reported (*37*). Hepatocytes were isolated from liver tissue from donors undergoing partial hepatectomy and were obtained with written informed consent approved by the Ethics Commission of Hannover Medical School (Ethik-Kommission der MHH, no. 252-2008). Again, supplemented HCM media (Lonza) were used to maintain primary hepatocytes in culture.

HCV infection assays

Initial HCV infection screening of murine hits using F-luc reporter HCV (Jc1) were conducted in 96-well plates (three technical replicates per condition) at MOI 0.1. Subsequent characterization was performed using R-luc reporter HCV (Jc1), again conducted in 96-well plates (three technical replicates per condition) at MOI 0.05. A minimum of three biological replicates were performed for all experiments. For HCV infection of plated murine hepatocytes, 5×10^5 $TCID_{50}$ units per six-well dish were used for WT Jc1 or p100pop virus. Viral supernatant was collected each day and replaced with fresh HCM media containing 10 μM ruxolitinib (AdipoGen, Leistel, Switzerland). The viral supernatants were then tested for infectious viral particle production using the $TCID_{50}$ assay.

Immunofluorescence and immunohistochemistry staining

Immunofluorescence and imaging of PMHs and Huh-7.5 cells overexpressing restriction factors were performed as follows. PMHs were seeded on collagen-coated glass coverslips in 24-well dishes. Huh-7.5 cells overexpressing murine *Cd302* or *Cr1l* were seeded on uncoated glass coverslips (5×10^4 cells per well) and grown until they reached about 80% confluence. Fixation was achieved by incubating the cells in chilled (4°C) 95% ethanol + 5% acetic acid for 10 min at room temperature. After two washes in PBS, cells were permeabilized for 10 min at room temperature in PBS + 0.1% Triton X-100 and rinsed twice again in PBS. To block potential nonspecific antibody binding, coverslips were incubated in a 5% solution of goat serum in PBS for 1 hour at room temperature. To detect murine Cd302, 5 μg/ml of an α-Cd302 monoclonal (Cd302/Clec13a; R&D Systems, rat IgG1) was used. To detect murine Cr1l, a polyclonal antibody solution at a concentration of 2 μg/ml (Crry M180; Santa Cruz Biotechnology, rabbit IgG1) was used. Incubation of these solutions was performed at room temperature for 1 hour or overnight at 4°C. After three washes in PBS, the primary antibodies were detected by fluorophore-conjugated anti-rat [Alexa Fluor 488 rabbit anti-rat immunoglobulin G (IgG); Life Technologies] and anti-rabbit [Alexa Fluor 568 donkey anti-rabbit IgG (H + L), Invitrogen] antibodies, respectively, at a concentration of 2 μg/ml in blocking solution for 1 hour at room temperature and protected from light. After washing off excess secondary antibodies with PBS twice for 5 min, staining of the nuclei was performed using a 0.5-μg/ml 4′,6-diamidino-2-phenylindole (DAPI) solution in H_2O. One final wash in H_2O was then followed by mounting of the coverslips in ProLong Gold Antifade Mountant (Thermo Fisher Scientific) and drying overnight at room temperature protected from

light. For imaging, an inversed confocal laser scanning microscope (Olympus FluoView 1000) with a ×100 magnification objective was used with FluoView 1000 imaging software (Olympus). Microscope settings, including laser intensity and exposure time, were identical for the target protein (Cd302 or Cr1l), the isotype control, and the secondary only control, respectively.

Matrigel-polarized organoids were infected with DiD-HCV, incubated on ice for an hour, then transferred to 37°C (time of temperature shift: $t = 0$), and fixed in 3.6% paraformaldehyde (PFA) at various points post-temperature shift. Cells were fixed for 20 min in PFA, permeabilized with 1% Triton X-100/PBS for 10 min, washed with 0.1 M glycine in PBS three times for 10 min each, and then incubated in blocking solution for 2 hours (wash buffer: 0.1% bovine serum albumin, 0.2% Triton X-100, and 0.005% Tween 20 in PBS + 20% goat serum). Samples were incubated at 4°C overnight with anti–ZO-1 antibody (1:500; Invitrogen) and then allowed to reform at room temperature for 10 min. Samples were washed three times for 20 min each time, with wash buffer, and then incubated for 1 hour at room temperature with Alexa Fluor–conjugated secondary antibody (488) in blocking solution. Coverslips were washed three times as above and then mounted on slides with DAPI prolong gold (Invitrogen). Slides were imaged using an Olympus Disk Scanning Unit Spinning Disc Confocal with a 100× numerical aperture 1.45 oil-immersion objective and Hamamatsu back thinned electron multiplying charge-coupled device camera; images were captured using SlideBook imaging software; intensification was set to 255, and z-stacks of the organoids were acquired with 0.3-μm slices. After acquisition, images were quantified for colocalization in ImageJ with RGB profiler (C. Laummonerie) and colocalization highlighter. Images were selected from z-stack slices, separated into channels, adjusted for contrast and brightness, smoothed, and finally reassembled.

For the detection of Cr1l (Crry) in formalin-fixed and paraffin-embedded murine tissue, the antibody sc30214 (Santa Cruz Biotechnology) was diluted 1:400, and antigen retrieval was performed by 20′ microwave/citrate cooking. As a negative control, the primary antibody was replaced in the same concentration with rabbit serum, and for all slides, a biotinylated goat anti-rabbit secondary antibody was used. For visualization, 3,3′-diaminobenzidine was applied.

Flow cytometry

A confluent monolayer of cells was detached using trypsin with the exception of PMHs, which were detached using EDTA (1 mM). Cells were pelleted and subsequently resuspended in FACS buffer (1% FCS in PBS). Approximately 1×10^6 Huh-7.5 cells or CHO-745 cells overexpressing mouse restriction factors or PMHs endogenously expressing these factors were stained for 30 min at 4°C with unconjugated primary monoclonal antibodies specific for Cd302 (Cd302/Clec13a; R&D Systems, rat IgG1) and Cr1l (Crry M180; Santa Cruz Biotechnology, rabbit IgG1 or anti-Cr1l biorbyt and rabbit IgG) diluted in FACS buffer to 1.6 μg/ml. To analyze the endogenous expression of human receptors present on Huh 7.5 cells, primary unconjugated antibodies specific for scavenger receptor class B type 1 (Novus; polyclonal rabbit antibody), Claudin 1 (R&D Systems; rat IgG), and OCLN (Life technologies; mouse IgG) were diluted in FACS buffer to 20, 10, and 1 μg/ml, respectively. For CD81, directly coupled antibody to fluorescein isothiocyanate (FITC) was used (BD Pharmingen, JS-81). Subsequently, cells were washed with FACS buffer thrice, and bound antibodies were detected by incubation for 30 min at 4°C with specific secondary antibody conjugated to an Alexa Fluor (Life Technologies), namely, anti-mouse Alexa Fluor 488, anti-rabbit Alexa Fluor 647, and anti-mouse Alexa Fluor 647 at a dilution of 1:1000 in FACS buffer and rat-specific secondary antibody conjugated to phycoerythrin (eBioscience) at a dilution of 1:200 in FACS buffer. The following isotype controls were used: rat isotype IgG 1 (R&D Systems), rabbit polyclonal (Abcam), and isotype FITC mouse IgG1κ (BD Pharmingen) at the same concentration as primary antibodies. Stained cells were washed with FACS buffer thrice, resuspended in FACS buffer, and analyzed immediately using an Accuri C6 cytometer (BD Biosciences), and data were analyzed using FlowJo software (Tree Star).

Immunoprecipitation

The Huh-7.5 N-HA-HA-L-Cd302/Cr1l cell line was obtained by lentiviral transduction of Huh-7.5 cells with the pWPI-N-HA-HA-L-Cd302 plasmid, selection with blasticidin (5 μg/ml) and subsequent lentiviral transduction of the pWPI-Cr1l plasmid, followed by a double selection with blasticidin and puromycin (2.5 μg/ml). To test the interaction between Cd302 and Cr1l, half a confluent 15-cm dish of Huh-7.5/empty, Huh-7.5/Cr1l, or Huh-7.5 N-HA-HA-L-Cd302/Cr1l cells was harvested by trypsinization and lysed in 250 μl of IP buffer [50 mM Hepes (pH 7.4), 150 mM NaCl, 1 mM $CaCl_2$, 10% glycerol, 1% NP-40, and complete EDTA-free protease inhibitor cocktail 1× (Roche no. 04 693 124 001)] for 30 min on ice. Cell nuclei were removed by centrifugation (10 min at 20,000*g*), and 5 μl of the supernatant was kept as an input for the Western blot. The anti-HA resin (Sigma-Aldrich; A2095) was washed twice in PBS (30 s at 12,000*g*), and 25 μl was used per IP. Cleared lysates and resin were incubated together overnight on a rotating wheel at 4°C. Afterward, the beads were washed twice quickly (no incubation time), twice with 5-min incubation periods on a rotating wheel, and once quickly with IP buffer (without protease inhibitor). After a final quick wash in water, the proteins were eluted in reducing Laemmli buffer (7 min at 70°C) and loaded on an SDS–polyacrylamide gel electrophoresis for separation and transfer on a polyvinylidene difluoride membrane. The membrane was probed with rat anti-Cd302 antibody (1/250) and rabbit anti-Cr1l antibody (1/250), followed by the secondary goat anti-rat IRDye 800CW and donkey anti-rabbit IRDye680RD (both at 1/15,000; LI-COR). Signal intensities were read with the Odyssey CLx imager (LI-COR).

RT-qPCR

Total cellular RNAs from cell lines or primary cells were isolated using a NucleoSpin RNA Kit (Macherey Nagel) according to the manufacturer's instructions. Total RNA concentrations were quantified using a NanoDrop spectrophotometer (PEQLAB). Subsequently, 500 ng to 1 μg of total RNA was reverse-transcribed into cDNA using a PrimeScript First Strand cDNA Synthesis Kit (Takara) in accordance with the kit instructions. Reactions were performed in triplicate. Subsequent qPCR of cDNAs was performed using ×2 SYBR MasterMix (Takara) and the LightCycler 480 system (Roche). Validated primer pairs for all mRNAs were taken from PrimerBank (https://pga.mgh.harvard.edu/primerbank/). For quantification of fold regulation in gene expression, calculations were performed using the $\Delta\Delta_{CT}$ method (QIAGEN Data Analysis Center: https://www.qiagen.com/de/shop/genes-and-pathways/data-analysis-center-overview-page/). For normalization, *ACTB* and *HPRT* were used as reference genes.

Western blotting

Cells were washed with PBS and lysed in radioimmunoprecipitation buffer [0.3 M NaCl, 20 mM tris-HCl (pH 8), 1% sodium deoxycholate, 0.1% SDS, and 1% Triton X-100] for 30 min on ice. Total protein content was determined by Bradford assay. Equal protein amounts for each sample were mixed with 2× denaturing protein sample buffer [200 mM tris-HCl (pH 8.8), 5 mM EDTA, 0.1% bromophenol blue, 10% sucrose, 3.3% SDS, and 2% 2-mercaptoethanol], heated for 5 min at 98°C, loaded onto a 11% SDS gel, and resolved by electrophoresis. Subsequently, proteins were transferred to a polyvinylidene difluoride membrane, which was then blocked with 5% milk in PBS containing 0.5% Tween 20 for 1 hour at room temperature. The membrane was then incubated with either α-mCrry/mCr1l (1:250; Santa Cruz Biotechnology), α-mCd302 (1:250; R&D Systems), or α-β-actin (1:1000; Sigma-Aldrich) followed by incubation with secondary antibody coupled to horseradish peroxidase (Sigma-Aldrich). Bound antibodies were detected with the ECL Plus Detection System (GE Healthcare).

HCV pseudoparticles

Retroviral pseudoparticles were generated with surface glycoproteins derived from HCV E1E2 (isolates Con1, genotype 1b, or UKN2B2.8, genotype 2b) or an empty vector as negative control (pcDNA EMPTY). Packaging construct pHIT60 encoding MLV gag/pol was cotransfected with the retroviral vector (pRV-F-Luc) and the individual envelope expression constructs using polyethylenimine (PEI) (Polyplus, Illkirch, France). Twenty-four hours later, sodium butyrate (10 mM) was added to transfected cells and incubated for 6 to 8 hours. At 48 hours after transfection, virus-containing culture fluids were harvested, filtered through a 0.45-μm pore size filter (VWR International, USA), and used to inoculate target cells.

HCV core enzyme-linked immunosorbent assay

Murine hepatocytes plated in six-well dishes were harvested after infection via aspiration of media, washed three times in PBS, and lysed via addition of 300 μl of 1% Triton X-100 in PBS with added protease inhibitor (Roche). Lysates were subsequently diluted in 1% Triton X-100 in PBS, and cell-associated HCV core was quantified by an automated chemiluminescent microparticle immunoassay (Architect HCV Ag, Abbott, Germany).

Phylogenetic analysis

Phylogenetic analysis of mammalian *Cd302* sequences was performed using the maximum likelihood method implemented in MEGA7 (*38*) based on the data-specific model. The significance of groupings was assessed using the bootstrap approach with 1000 pseudoreplicates performed. The tree with the highest log likelihood is presented, with significant bootstrap values (70%) assigned to the corresponding branch. The tree was generated under a GTR + Γ + I model of substitution whereby discrete Gamma distribution (Γ) was used to model evolutionary rate differences among sites (four rate categories). The proportion of invariant sites (I) was also incorporated into the reconstruction. The phylogeny is drawn to scale, with branch lengths proportional to the number of substitutions per site. All positions containing gaps and missing data were eliminated from the analysis. The dataset incorporated *Cd302* sequences from 24 species, and a total of 603 nucleotide positions were included in the final analysis.

Canonical pathway analysis

Canonical pathway analyses were performed using IPA (QIAGEN). Data input consisted of an Excel sheet containing Ensembl identifiers, *P* values, FDR *P* values, fold change, and log fold change values for genes, as previously determined with CLC Genomics Workbench. In general, default settings were used for all categories, but species was set to "human" for data from Huh-7.5 cells ectopically expressing murine factors and "mouse" for data from PMHs. FDR *P* value significance threshold was set to 0.05 for genes included in the subsequent analysis. *Z* scores were calculated on the basis of the expression fold change.

Generation of mouse lines

Mice with hepatocyte-specific expression of human occludin and Cd81 (hOC^{hep}, h*OCLN*$^{+/-}$ h*CD81*$^{+/-}$) were generated by breeding hOC^{con} mice with AlbCre mice (*39*). hOC^{con} mice comprise an inverted, Cre-activatable expression cassette for human occludin and CD81 and were generated upon Flp-based targeted integration of the Rosa26 locus (*40*) using the following targeting cassette: Fwt – *IPS-RFP* – P_{CAGGS}-loxL3-loxP-(h*OCLN*-IRES- h*CD81*)^{inv}-loxL3^{inv}-loxP^{inv} – IRES – F5. Knockout of *Cd302* (*Cd302*$^{-/-}$) was achieved by CRISPR-Cas9–mediated excision of 40 bp including the initiation codon (c – 29) – (c + 11) in C57BL/6 zygotes using guide RNA target sites CACCCGACAAGCACCGCCCC and TGCACTCTCCGGGGCGCGGC, applying a previously published protocol (*41*). hOC^{hep} *Cd302*$^{-/-}$ animals were generated by breeding. Genetically modified mice were generated with the approval of the ethical board of the Lower Saxony State Office for Consumer Protection and Food Safety, Oldenburg, Germany.

CHO binding assay

CHO-745 cells were either left untransfected or PEI-transfected with pWPI-*SCARB1*, pWPI-*mCd302*, pWPI-*mCr1l*, or both pWPI-*mCd302* and pWPI-*mCr1l* together. Cell surface expression levels were analyzed 48 hours after transfection using FACS. At 48 hours after transfection, CHO-745 cells were incubated with HCVcc (Jc1) particles for 2 hours at 37°C. After binding, the cells were washed extensively with PBS, total RNA–isolated, and HCV RNA–quantified using RT-qPCR.

In vivo infections

hOC^{hep} or hOC^{hep} *Cd302*$^{-/-}$ mice were inoculated intrasplenically with 100 μl of concentrated DMEM containing 1.2×10^7 $TCID_{50}$ units of HCV p100pop virus. Ruxolitinib treatment was orally administered every 8 to 12 hours (starting 4 hours before infection) at a dose of 100 mg/kg, and ruxolitinib (Ambeed, IL, USA) was dissolved in 20% dimethyl sulfoxide (DMSO) and 50% PEG 400 (seven doses for animals tested for 3 days and 13 doses for animals tested for 5 days). At the end of each experiment, animals were euthanized, and blood and liver samples were processed for further analysis. All procedures were performed according to European and Belgian legislation and were approved by the Animal Ethics Committee of the Faculty of Medicine and Health Sciences of Ghent University. Snap-frozen whole or partial livers from individual mice were homogenized in RA1 lysis buffer from the Macherey Nagel NucleoSpin RNA Isolation kit at a concentration of 100 mg/ml. Total RNA extraction was then performed on 350 μl according to the manufacturer's instructions. To further enrich viral RNA, an HCV capture assay was performed whereby 10 μg of extracted total RNA was diluted in 200 μl of TEN buffer [10 mM tris-HCl (pH 8.0), 1 mM EDTA, and 100 mM NaCl] and incubated for 5 min at 75°C with subsequent addition of 0.5 μg of HCV-specific biotinylated capture DNA (BIOTEG-AAG

TAT ACT CCG CCA ACG ATC TGG CCG CCG) followed by vortexing and further incubation for 5 min at 65°C. Meanwhile, μMACS columns were equilibrated according to the manufacturer's instructions (μMACS Streptavidin Kit, Miltenyi Biotec). One hundred microliters of μMACS streptavidin microbeads was then added to the mix and incubated for further 2 min at 65°C. The solution was then added to the μMACS columns and washed with 5 × 200 μl with TE buffer [10 mM tris-HCl (pH 8.0) and 1 mM EDTA], and captured RNA was then eluted with 150 μl of H_2O preheated to 80°C. Drops 2 to 4 were collected (approximately 50 μl) for analysis by RT-qPCR. Captured RNA from the liver samples were analyzed by RT-qPCR using the Roche LightCycler 480 RNA Master Hydrolysis Probes kit (Roche), primers (5′-TCTGCGGAACCGGTGAGTA-3′ and 5′-GGGCATAGAGTGGGTTTATCCA-3′) and probe (5′-6FAM-AAAGGACCCAGTCTTCCCGGCAA-TMR-3′), according to the manufacturer's conditions.

Cd302 structure modeling

A homology model of the extracellular domain of mCd302 was generated on the basis of the NMR structure of the hCD302 extracellular domain [Protein Data Bank (PDB) 2NAN] using the Phyre2 web server (*42*). Nonconserved residues were mapped on the surface of mCd302 according to a pairwise sequence alignment obtained via Clustal Omega (*43*). Structure figures were prepared with PyMOL (The PyMOL Molecular Graphics System, version 1.8.0.3, Schrödinger, LLC).

Statistical analysis

Statistical tests were performed in GraphPad Prism v8.0 on data generated from biological experiments, with appropriate correction for multiple comparisons: $^{****}P < 0.0001$, $^{***}P < 0.001$, $^{**}P < 0.01$, and $^{*}P < 0.05$. Statistical analysis of DEGs from RNA-seq experiments was performed in CLC Genomics Workbench with FDR or Bonferroni correction for multiple comparisons.

SUPPLEMENTARY MATERIALS

Supplementary material for this article is available at http://advances.sciencemag.org/cgi/content/full/6/45/eabd3233/DC1

View/request a protocol for this paper from *Bio-protocol*.

REFERENCES AND NOTES

1. World Health Organization, *Global Hepatitis Report, 2017* (World Health Organization, 2017).
2. World Health Organizatioin, *Hepatitis C* (2020); https://www.who.int/news-room/fact-sheets/detail/hepatitis-c.
3. S. L. Sawyer, N. C. Elde, A cross-species view on viruses. *Curr. Opin. Virol.* **2**, 561–568 (2012).
4. E. V. Mesev, R. A. LeDesma, A. Ploss, Decoding type I and III interferon signalling during viral infection. *Nat. Microbiol.* **4**, 914–924 (2019).
5. C. J. Warren, S. L. Sawyer, How host genetics dictates successful viral zoonosis. *PLOS Biol.* **17**, e3000217 (2019).
6. S. Pfaender, J. M. V. Cavalleri, S. Walter, J. Doerrbecker, B. Campana, R. J. P. Brown, P. D. Burbelo, A. Postel, K. Hahn, Anggakusuma, N. Riebesehl, W. Baumgärtner, P. Becher, M. H. Heim, T. Pietschmann, K. Feige, E. Steinmann, Clinical course of infection and viral tissue tropism of hepatitis C virus-like nonprimate hepaciviruses in horses. *Hepatology* **61**, 447–459 (2015).
7. S. Pfaender, S. Walter, E. Grabski, D. Todt, J. Bruening, I. Romero-Brey, T. Gather, R. J. P. Brown, K. Hahn, C. Puff, V. M. Pfankuche, F. Hansmann, A. Postel, P. Becher, V. Thiel, U. Kalinke, B. Wagner, R. Bartenschlager, W. Baumgärtner, K. Feige, T. Pietschmann, J. M. V. Cavalleri, E. Steinmann, Immune protection against reinfection with nonprimate hepacivirus. *Proc. Natl. Acad. Sci. U.S.A.* **114**, E2430–E2439 (2017).
8. E. Billerbeck, R. Wolfisberg, U. Fahnøe, J. W. Xiao, C. Quirk, J. M. Luna, J. M. Cullen, A. S. Hartlage, L. Chiriboga, K. Ghoshal, W. I. Lipkin, J. Bukh, T. K. H. Scheel, A. Kapoor, C. M. Rice, Mouse models of acute and chronic hepacivirus infection. *Science* **357**, 204–208 (2017).
9. S. Trivedi, S. Murthy, H. Sharma, A. S. Hartlage, A. Kumar, S. V. Gadi, P. Simmonds, L. V. Chauhan, T. K. H. Scheel, E. Billerbeck, P. D. Burbelo, C. M. Rice, W. I. Lipkin, K. Vandegrift, J. M. Cullen, A. Kapoor, Viral persistence, liver disease, and host response in a hepatitis C-like virus rat model. *Hepatology* **68**, 435–448 (2018).
10. A. Frentzen, Anggakusuma, E. Gürlevik, K. Hueging, S. Knocke, C. Ginkel, R. J. P. Brown, M. Heim, M. T. Dill, A. Kröger, U. Kalinke, L. Kaderali, F. Kuehnel, T. Pietschmann, Cell entry, efficient RNA replication, and production of infectious hepatitis C virus progeny in mouse liver-derived cells. *Hepatology* **59**, 78–88 (2014).
11. M. Dorner, J. A. Horwitz, B. M. Donovan, R. N. Labitt, W. C. Budell, T. Friling, A. Vogt, M. T. Catanese, T. Satoh, T. Kawai, S. Akira, M. Law, C. M. Rice, A. Ploss, Completion of the entire hepatitis C virus life cycle in genetically humanized mice. *Nature* **501**, 237–241 (2013).
12. M. Dorner, J. A. Horwitz, J. B. Robbins, W. T. Barry, Q. Feng, K. Mu, C. T. Jones, J. W. Schoggins, M. T. Catanese, D. R. Burton, M. Law, C. M. Rice, A. Ploss, A genetically humanized mouse model for hepatitis C virus infection. *Nature* **474**, 208–211 (2011).
13. Z. Chen, R. L. Simeon, K. Chockalingam, C. M. Rice, Creation and characterization of a cell-death reporter cell line for hepatitis C virus infection. *Antiviral Res.* **86**, 220–223 (2010).
14. P. Metz, E. Dazert, A. Ruggieri, J. Mazur, L. Kaderali, A. Kaul, U. Zeuge, M. P. Windisch, M. Trippler, V. Lohmann, M. Binder, M. Frese, R. Bartenschlager, Identification of type I and type II interferon-induced effectors controlling hepatitis C virus replication. *Hepatology* **56**, 2082–2093 (2012).
15. M. Saeed, U. Andreo, H.-Y. Chung, C. Espiritu, A. D. Branch, J. M. Silva, C. M. Rice, *SEC14L2* enables pan-genotype HCV replication in cell culture. *Nature* **524**, 471–475 (2015).
16. Y. Baktash, A. Madhav, K. E. Coller, G. Randall, Single particle imaging of polarized hepatoma organoids upon hepatitis C virus infection reveals an ordered and sequential entry process. *Cell Host Microbe* **23**, 382–394.e5 (2018).
17. J. D. Esko, T. E. Stewart, W. H. Taylor, Animal cell mutants defective in glycosaminoglycan biosynthesis. *Proc. Natl. Acad. Sci. U.S.A.* **82**, 3197–3201 (1985).
18. M. J. Evans, T. von Hahn, D. M. Tscherne, A. J. Syder, M. Panis, B. Wölk, T. Hatziioannou, J. A. McKeating, P. D. Bieniasz, C. M. Rice, Claudin-1 is a hepatitis C virus co-receptor required for a late step in entry. *Nature* **446**, 801–805 (2007).
19. E. Scarselli, H. Ansuini, R. Cerino, R. M. Roccasecca, S. Acali, G. Filocamo, C. Traboni, A. Nicosia, R. Cortese, A. Vitelli, The human scavenger receptor class B type I is a novel candidate receptor for the hepatitis C virus. *EMBO J.* **21**, 5017–5025 (2002).
20. M. Kato, S. Khan, E. d'Aniello, K. J. McDonald, D. N. J. Hart, The novel endocytic and phagocytic C-Type lectin receptor DCL-1/CD302 on macrophages is colocalized with F-actin, suggesting a role in cell adhesion and migration. *J. Immunol.* **179**, 6052–6063 (2007).
21. T.-H. Lo, P. A. Silveira, P. D. Fromm, N. D. Verma, P. A. Vu, F. Kupresanin, R. Adam, M. Kato, V. C. Cogger, G. J. Clark, D. N. J. Hart, Characterization of the expression and function of the C-type lectin receptor CD302 in mice and humans reveals a role in dendritic cell migration. *J. Immunol.* **197**, 885–898 (2016).
22. I. Rusinova, S. Forster, S. Yu, A. Kannan, M. Masse, H. Cumming, R. Chapman, P. J. Hertzog, Interferome v2.0: An updated database of annotated interferon-regulated genes. *Nucleic Acids Res.* **41**, D1040–D1046 (2013).
23. K. Li, Z. Chen, N. Kato, M. Gale Jr., S. M. Lemon, Distinct poly(I-C) and virus-activated signaling pathways leading to interferon-β production in hepatocytes. *J. Biol. Chem.* **280**, 16739–16747 (2005).
24. R. W. Meredith, J. E. Janečka, J. Gatesy, O. A. Ryder, C. A. Fisher, E. C. Teeling, A. Goodbla, E. Eizirik, T. L. L. Simão, T. Stadler, D. L. Rabosky, R. L. Honeycutt, J. J. Flynn, C. M. Ingram, C. Steiner, T. L. Williams, T. J. Robinson, A. Burk-Herrick, M. Westerman, N. A. Ayoub, M. S. Springer, W. J. Murphy, Impacts of the cretaceous terrestrial revolution and KPg extinction on mammal diversification. *Science* **334**, 521–524 (2011).
25. A. N. Zelensky, J. E. Gready, The C-type lectin-like domain superfamily. *FEBS J.* **272**, 6179–6217 (2005).
26. E. Pospíšilová, D. Kavan, P. Novák, J. Chmelík, ^{1}H, ^{13}C and ^{15}N resonance assignments of human DCL-1 (CD302) extracellular domain. *Biomol. NMR Assign.* **10**, 189–192 (2016).
27. C. Perales, N. M. Beach, I. Gallego, M. E. Soria, J. Quer, J. I. Esteban, C. Rice, E. Domingo, J. Sheldon, Response of hepatitis C virus to long-term passage in the presence of alpha interferon: Multiple mutations and a common phenotype. *J. Virol.* **87**, 7593–7607 (2013).
28. C. Xu, D. Mao, V. M. Holers, B. Palanca, A. M. Cheng, H. Molina, A critical role for murine complement regulator crry in fetomaternal tolerance. *Science* **287**, 498–501 (2000).
29. F. Ma, S.-Y. Liu, B. Razani, N. Arora, B. Li, H. Kagechika, P. Tontonoz, V. Núñez, M. Ricote, G. Cheng, Retinoid X receptor α attenuates host antiviral response by suppressing type I interferon. *Nat. Commun.* **5**, 5494 (2014).
30. G. Levy, N. Habib, M. A. Guzzardi, D. Kitsberg, D. Bomze, E. Ezra, B. E. Uygun, K. Uygun, M. Trippler, J. F. Schlaak, O. Shibolet, E. H. Sklan, M. Cohen, J. Timm, N. Friedman,

Y. Nahmias, Nuclear receptors control pro-viral and antiviral metabolic responses to hepatitis C virus infection. *Nat. Chem. Biol.* **12**, 1037–1045 (2016).
31. S. Mayer, M.-K. Raulf, B. Lepenies, C-type lectins: Their network and roles in pathogen recognition and immunity. *Histochem. Cell Biol.* **147**, 223–237 (2017).
32. J. Z. Levin, M. Yassour, X. Adiconis, C. Nusbaum, D. A. Thompson, N. Friedman, A. Gnirke, A. Regev, Comprehensive comparative analysis of strand-specific RNA sequencing methods. *Nat. Methods* **7**, 709–715 (2010).
33. K. E. Coller, K. L. Berger, N. S. Heaton, J. D. Cooper, R. Yoon, G. Randall, RNA interference and single particle tracking analysis of hepatitis C virus endocytosis. *PLOS Pathog.* **5**, e1000702 (2009).
34. P. Shukla, H. T. Nguyen, K. Faulk, K. Mather, U. Torian, R. E. Engle, S. U. Emerson, Adaptation of a genotype 3 hepatitis E virus to efficient growth in cell culture depends on an inserted human gene segment acquired by recombination. *J. Virol.* **86**, 5697–5707 (2012).
35. V. L. Dao Thi, Y. Debing, X. Wu, C. M. Rice, J. Neyts, D. Moradpour, J. Gouttenoire, Sofosbuvir inhibits hepatitis E virus replication in vitro and results in an additive effect when combined with ribavirin. *Gastroenterology* **150**, 82–85.e4 (2016).
36. M. Rothe, I. Rittelmeyer, M. Iken, U. Rüdrich, A. Schambach, S. Glage, M. P. Manns, C. Baum, M. Bock, M. Ott, U. Modlich, Epidermal growth factor improves lentivirus vector gene transfer into primary mouse hepatocytes. *Gene Ther.* **19**, 425–434 (2012).
37. M. Kleine, M. Riemer, T. Krech, D. DeTemple, M. D. Jäger, F. Lehner, M. P. Manns, J. Klempnauer, J. Borlak, H. Bektas, F. W. Vondran, Explanted diseased livers—A possible source of metabolic competent primary human hepatocytes. *PLOS ONE* **9**, e101386 (2014).
38. S. Kumar, G. Stecher, K. Tamura, MEGA7: Molecular evolutionary genetics analysis version 7.0 for bigger datasets. *Mol. Biol. Evol.* **33**, 1870–1874 (2016).
39. C. Postic, M. Shiota, K. D. Niswender, T. L. Jetton, Y. Chen, J. M. Moates, K. D. Shelton, J. Lindner, A. D. Cherrington, M. A. Magnuson, Dual roles for glucokinase in glucose homeostasis as determined by liver and pancreatic β cell-specific gene knock-outs using Cre recombinase. *J. Biol. Chem.* **274**, 305–315 (1999).
40. U. Sandhu, M. Cebula, S. Behme, P. Riemer, C. Wodarczyk, D. Metzger, J. Reimann, R. Schirmbeck, H. Hauser, D. Wirth, Strict control of transgene expression in a mouse model for sensitive biological applications based on RMCE compatible ES cells. *Nucleic Acids Res.* **39**, e1 (2011).
41. V. T. Chu, T. Weber, R. Graf, T. Sommermann, K. Petsch, U. Sack, P. Volchkov, K. Rajewsky, R. Kühn, Efficient generation of *Rosa26* knock-in mice using CRISPR/Cas9 in C57BL/6 zygotes. *BMC Biotechnol.* **16**, 4 (2016).
42. L. A. Kelley, S. Mezulis, C. M. Yates, M. N. Wass, M. J. E. Sternberg, The Phyre2 web portal for protein modeling, prediction and analysis. *Nat. Protoc.* **10**, 845–858 (2015).
43. F. Sievers, A. Wilm, D. Dineen, T. J. Gibson, K. Karplus, W. Li, R. Lopez, H. McWilliam, M. Remmert, J. Söding, J. D. Thompson, D. G. Higgins, Fast, scalable generation of high-quality protein multiple sequence alignments using Clustal Omega. *Mol. Syst. Biol.* **7**, 539 (2011).

Acknowledgments: We thank the following people for their contribution of reagents and infrastructure that greatly enhanced this study: HZI Braunschweig GMAK facility, including R. Geffers, M. Jarek, S. Bhuju, and M. Scharfe for generating RNA-seq data; HZI Braunschweig TGSM transgenic for generation of genetically modified mice and the Central Animal Facility for mouse housing; the MHH Diagnostics and T. Schultz and his team for diagnostic core ELISA; J. Bukh for the pan-genotypic panel of JFH-1–based chimeras; V. Thiel for hCoV 229E; P. Bieniasz for the lentiviral vector pV1; M. Evans for sharing his library generation protocol; Z. Chen for n4mBid cells; J. Ball for HCV E1E2 plasmid UKN2B2.1; M. Heim for providing IFN-treated mouse livers; O. Dittrich-Breiholz at the Research Core Unit Genomics, MHH, for access to IPA; and all members, past and present, of Experimental Virology Group at Twincore for useful discussion, including K. Hueging, P. Perin, and A. Frentzen for technical contributions. **Funding:** A.P. was funded by grants from the National Institute of Allergy and Infectious Diseases (R01AI107301-06), the American Cancer Society (RSG-15-048-01-MPC), and the Burroughs Wellcome Fund Award for Investigators in Pathogenesis program. P.M. was supported by grants from the Research Foundation—Flanders (FWO-Vlaanderen; projects G047417N and VirEOS 30981113). T.Kr. was funded by the Deutsche Forschungsgemeinschaft (DFG, German Research Foundation) within project B10 of CRC 900—project 158989968. T.P. was funded by a grant from the European Research Council ERC-2011-StG_281473-(VIRAFRONT). He is also funded by the Deutsche Forschungsgemeinschaft (DFG, German Research Foundation) under the Germany's Excellence Strategy—EXC 2155 "RESIST"—project ID 39087428. He receives support through the German Center of Infection Research via the Delphi grant and from the National Institute of Allergy and Infectious Diseases (R01AI107301). R.J.P.B. was funded by BMG grant 1-2516-FSB-416. Deutsche Forschungsgemeinschaft (DFG, German Research Foundation)—SFB900 project C7 serial number: 158989968. Funding dates: 1 July 2018 to 30 June 2022. DFG Deutsche Forschungsgemeinschaft (DFG, German Research Foundation) serial number: GE 2145/3-2. Funding dates: 1 April 2017 to 31 March 2020 (no cost extension until 30 June 2021). **Author contributions:** Conceptualization: R.J.P.B. and T.P. Methodology: R.J.P.B., T.P., G.R., Y.B., N.G., and D.W. Validation: R.J.P.B., B.T., J.S., T.Kh., Anggakusuma, G.V., R.W., S.J., Y.Z., S.S., D.B., K.W., V.H., C.L., G.R., Y.B., V.L.D.T., E.M., M.S., N.G., D.W., and T.P. Formal analysis: R.J.P.B., B.T., D.T., G.G., T.Kr., L.J.S., C.M., C.L., and T.P. Investigation: R.J.P.B., B.T., J.S., T.Kh., Anggakusuma, G.V., R.W., S.J., Y.Z., S.S., D.B., K.W., M.E., C.G., Q.Y., V.H., A.W.T., C.P.M., Y.B., V.L.D.T., E.M., M.S., L.V., and N.G. Resources: E.S., M.O., F.W.R.V., W.B., Z.I., M.S., A.P., P.M., D.W., and C.M.R. Data curation: R.J.P.B., B.T., and C.M. Writing—original draft: R.J.P.B. and T.P. Writing—review and editing: B.T., E.S., T.Kr., A.P., E.M., M.S., P.M., D.W., and C.M.R. Visualization: R.J.P.B., B.T., D.T., T.Kr., L.J.S., and T.P. Supervision: R.J.P.B. and T.P. Project administration: R.J.P.B. and T.P. Funding acquisition: R.J.P.B., A.P., P.M., T.Kr., and T.P. **Competing interests:** C.M.R. is a member of the Twincore Scientific Advisory Board, an unpaid advisory position. R.J.P.B. and T.P. are inventors on a pending patent application related to this work filed by Twincore, Zentrum für Experimentelle und Klinische Infektionsforschung GMBH [EP3463411A1 (Europe) and US2019/0297860A1 (USA), 02 June 2016]. The authors declare that they have no other competing interests. **Data and materials availability:** All data needed to evaluate the conclusions in the paper are present in the paper and/or the Supplementary Materials. Additional data related to this paper may be requested from the authors. Raw and processed RNA-seq data generated in this study are submitted to the NCBI GEO database (GEO accession number GSE140591). RNA-seq data from Huh-7.5 cells transduced with a control EMTPY lentivirus are reported in Tegtmeyer and Vieyres (manuscript in revision: accession number GSE132548). Transgenic knockout mice generated in this study are available from the authors under a material transfer agreement.

Submitted 16 June 2020
Accepted 21 September 2020
Published 4 November 2020
10.1126/sciadv.abd3233

Citation: R. J. Brown, B. Tegtmeyer, J. Sheldon, T. Khera, Anggakusuma, D. Todt, G. Vieyres, R. Weller, S. Joecks, Y. Zhang, S. Sake, D. Bankwitz, K. Welsch, C. Ginkel, M. Engelmann, G. Gerold, E. Steinmann, Q. Yuan, M. Ott, F. W. R. Vondran, T. Krey, L. J. Ströh, C. Miskey, Z. Ivics, V. Herder, W. Baumgärtner, C. Lauber, M. Seifert, A. W. Tarr, C. P. McClure, G. Randall, Y. Baktash, A. Ploss, V. L. D. Thi, E. Michailidis, M. Saeed, L. Verhoye, P. Meuleman, N. Goedecke, D. Wirth, C. M. Rice, T. Pietschmann, Liver-expressed *Cd302* and *Cr1l* limit hepatitis C virus cross-species transmission to mice. *Sci. Adv.* **6**, eabd3233 (2020).

Science Advances

Liver-expressed *Cd302* and *Cr1l* limit hepatitis C virus cross-species transmission to mice

Richard J. P. Brown, Birthe Tegtmeyer, Julie Sheldon, Tanvi Khera, Anggakusuma, Daniel Todt, Gabrielle Vieyres, Romy Weller, Sebastian Joecks, Yudi Zhang, Svenja Sake, Dorothea Bankwitz, Kathrin Welsch, Corinne Ginkel, Michael Engelmann, Gisa Gerold, Eike Steinmann, Qinggong Yuan, Michael Ott, Florian W. R. Vondran, Thomas Krey, Luisa J. Ströh, Csaba Miskey, Zoltán Ivics, Vanessa Herder, Wolfgang Baumgärtner, Chris Lauber, Michael Seifert, Alexander W. Tarr, C. Patrick McClure, Glenn Randall, Yasmine Baktash, Alexander Ploss, Viet Loan Dao Thi, Eleftherios Michailidis, Mohsan Saeed, Lieven Verhoye, Philip Meuleman, Natascha Goedecke, Dagmar Wirth, Charles M. Rice and Thomas Pietschmann

Sci Adv **6** (45), eabd3233.
DOI: 10.1126/sciadv.abd3233